Original paper

Discorhabdin alkaloids from Antarctic *Latrunculia* spp. sponges as a new class of cholinesterase inhibitors

Tanja Botić[a], Andrea Defant[b], Pietro Zanini[b], Monika Cecilija Žužek[c], Robert Frangež[c], Dorte Janussen[d], Daniel Kersken[d], Željko Knez[a], Ines Mancini*[b], Kristina Sepčić*[e]

[a]Laboratory for Separation Processes and Product Design, Faculty of Chemistry and Chemical Engineering, University of Maribor, Smetanova 17, 2000 Maribor, Slovenia

[b]Laboratory of Bioorganic Chemistry, Department of Physics, University of Trento, via Sommarive, 14, I-38123 Povo-Trento, Italy

[c]Institute of Preclinical Sciences, Veterinary Faculty, University of Ljubljana, Gerbičeva 60, Slovenia

[d]Marine Zoology Department, Senckenberg Research Institute and Nature Museum, Senckenberganlage 25, D-60325 Frankfurt am Main, Germany

[e]Department of Biology, Biotechnical Faculty, University of Ljubljana, Večna pot 111, 1000 Ljubljana, Slovenia

***Corresponding authors**:

kristina.sepcic@bf.uni-lj.si

ines.mancini@unitn.it

ABSTRACT

The brominated pyrroloiminoquinone alkaloids discorhabdins B, L and G and 3-dihydro-7,8-dehydrodiscorhabdin C, isolated from methanol extracts of two specimens of *Latrunculia* sp. sponges collected near the Antarctic Peninsula, are here demonstrated for the first time to be reversible competitive inhibitors of cholinesterases. They showed K_i for electric eel acetylcholinesterase of 1.6-15.0 μM, for recombinant human acetylcholinesterase of 22.8-98.0 μM, and for horse serum butyrylcholinesterase of 5.0-76.0 μM. These values are promising when compared to the current cholinesterase inhibitors used for treatment of patients with Alzheimer's disease, to counteract the acetylcholine deficiency in the brain. Good correlation was obtained between IC_{50} data and results by molecular docking calculation on the binding interactions within the acetylcholinesterase active site, which also indicated the moieties in discorhabdin structures involved. To avoid unwanted peripheral side effects that can appear in patients using some acetylcholinesterase inhibitors, electrophysiological experiments were carried out on one of the most active of these compounds, discorhabdin G, which confirmed that it had no detectable undesirable effects on neuromuscular transmission and skeletal muscle function. These findings are promising for development of cholinesterase inhibitors based on the scaffold of discorhabdins, as potential new agents for treatment of patients with Alzheimer's disease.

Keywords: Acetylcholinesterase inhibitor; Alzheimer's disease; Antarctic sponges; Discorhabdins; Molecular docking, Sponge metabolites.

Abbreviations: AChE, acetylcholinesterase; BChE, butyrylcholinesterase; eeAChE, electric eel acetylcholinesterase; ESI-MS, electrospray ionisation-mass spectrometry; hAChE, recombinant human acetylcholinesterase; HMBC, heteronuclear multiple bond coherence; HPLC, high performance liquid chromatography; NMR, nuclear magnetic resonance; PDB, protein data bank; TFA, trifluoracetic acid.

1. Introduction

Cancer and cardiovascular dysfunction are currently the most diffuse diseases in the developed world, followed by Alzheimer's disease. It is a progressive neurodegenerative disease that leads to gradual memory decline and loss of intellectual abilities, and is associated with behavioural disorders and personality change [1]. Alzheimer's disease is the most common type of dementia and because of the aging population; it has become an ever-increasing social and economic problem. Currently, there are some 46.8 million people around the world who live with Alzheimer's disease or some other kind of dementia, and this number is expected to double over the next 20 years [2]. Unfortunately, at present there is no treatment that can stop, or preferably reverse, the progression of this neurological disorder. With the current selection of therapeutic agents, it is only possible to slow the progression of the disease, and to reduce the symptomatology.

Patients diagnosed with Alzheimer's disease show the characteristic neurochemical deficit of the neurotransmitter acetylcholine, especially in the basal forebrain. This is a consequence of enhanced activity of their acetylcholinesterase (AChE; E.C. 3.1.1.7), an enzyme that is mainly located in nerve synapses and neuromuscular junctions, where it catalyses cleavage of acetylcholine. As well as decreasing the levels of acetylcholine, AChE is partially responsible for promotion of β-amyloid peptide aggregation, and the consequent formation of amyloid plaques [3, 4]. Clinical studies have shown that inhibition of AChE to decrease the rate of acetylcholine hydrolysis is a promising strategy in the therapy of Alzheimer's disease, as it can reverse the reduced cognition and aberrant behavioural functions associated with Alzheimer's disease [5]. Indeed, most of the currently available anti-Alzheimer's drugs are AChE inhibitors, the standard use of which is supported by clinical evidence [4, 6]. These inhibitors cannot reduce the rate of decline in the cognitive and functional capacities of patients with Alzheimer's disease, although over the long term, they can provide meaningful symptomatic benefits.

Alzheimer's disease is also associated with progressive increase in the activity of the related enzyme butyrylcholinesterase (BChE; E.C. 3.1.1.8). BChE is mainly located in the blood plasma [7], and it is assumed to serve as a 'back-up' for when AChE activity is compromised or absent, thus providing further support for and regulation of cholinergic transmission [8]. In this regard, AChE and BChE both represent interesting therapeutic targets for amelioration of the symptoms of Alzheimer's disease.

The US Food and Drug Administration has approved a number of drugs for the treatment of patients with Alzheimer's disease, which include the synthetic pharmaceuticals donepezil, rivastigmine, tacrine and galantamine. Galantamine was initially isolated from the common snowdrop, *Galanthus woronowii* [9], and it has contra-indications for therapeutic use due to heart problems, epilepsy, and gastrointestinal symptoms. This requires the search for new drugs for the treatment of Alzheimer's disease that have reduced side effects.

Other important commercially available plant-derived natural AChE inhibitors include physostigmine from the Calabar bean *Physostigma venenosum* [10] and huperzine A from the Chinese club moss *Huperzia serrata* [11]. In recent years, several AChE inhibitors have also been isolated from marine organisms, such as soft corals, molluscs, ascidians, and in particular, sponges (reviewed in Orhan et al. [12]). Indeed, nearly half of the marine natural bioactive compounds now derive from sponges, which are considered to be the most bio-prospective [13] and pharmacodiverse marine taxa [14].

Sponges from the genus *Latrunculia* have been recognized as sources of the discorhabdin alkaloids [15-17]. These metabolites are pigments with a very particular structure that is characterised by azacarbocyclic spirocyclohexanone and pyrroloiminoquinone units. Over 40 members of the discorhabdin classes have been reported to date, with these defined according to: (i) the presence of sulfur cross-linkage (discorhabdins A, B, D, I, K, L, Q, R, X); (ii) the presence of a methyl sulfide substituent (discorhabdins S, T, U); (iii) the absence of a sulphur atom (discorhabdins C, D, G, E, F, O, P); and (iv) the presence of a rare dimeric structure (discorhabdin W). The discorhabdins and discorhabdin-related alkaloids show a plethora of biological effects, which include strong cytotoxic, antimicrobial, antiviral, antimalarial, immunomodulatory, caspase-inhibitory, and feeding-deterrent activities [16]. Due to these biological properties, the isolation, structural determination, reactivity and synthesis of these alkaloids have attracted considerable attention [18].

In 1975, Nèeman et al. [19] reported on a structurally unidentified toxin that they isolated from the Red Sea sponge *Latrunculia magnifica* that showed strong BChE inhibition. More recently, Turk et al. [20] evaluated AChE-inhibitory effects of ethanolic extracts obtained from two specimens of Antarctic *Latrunculia* spp. sponges, namely *Latrunculia* cf. *lendenfeldi* and *Latrunculia* cf. *bocagei*. These extracts induced 50% inhibition of electric eel AChE (eeAChE) at concentrations of 1.3 ng and 9 ng dried extract/mL, respectively. Thus, the identification of the

metabolites responsible for these bioactivities and investigations into their mechanisms of action require further studies.

We initially report here on the isolation of four discorhabdins from methanol extracts of *Latrunculia* spp. sponges that were dredged from the deep Antarctic shelf in the Bransfield Strait near the Antarctic Peninsula in 2013. We further report on the evaluation of these metabolites as AChE inhibitors, with experimental data supported by docking calculations and related to their corresponding anti-BChE activities. One of the most active of these compounds, discorhabdin G, also underwent electrophysiological analysis to define any undesirable effects on neuromuscular transmission.

2. Results and Discussion

2.1. Isolation and structural characterisation of discorhabdin alkaloids 1-4

(+)-Discorhabdin G (**1** in Fig. 1) and (-)3-dihydro-7,8-dehydro discorhabdin C (**2** in Fig. 1) were isolated in pure form starting from a crude methanol extract of *L. biformis*. The first purification step was on a cyano HPLC column eluting with water/ methanol/ TFA (60:40:1, v/v/v). The fraction collected at 7 min underwent further preparative workup on an RP-18 column with acetonitrile/ water/ TFA (30:70:1, v/v/v), obtaining the fraction eluted at 11 min which was further purified on a cyano HPLC column by elution with acetonitrile/ water/ TFA (30:70:1, v/v/v), to give the pure discorhabdin G triflate salt (**1**) as a brown solid. Electrospray ionisation mass spectrometry (ESI-MS) spectra, recorded in positive ion mode by direct infusion from a methanolic solution, showed a double signal at *m/z* 384/ 386 in a 1:1 ratio, corresponding to the M^+ ion, which indicated the presence of one bromine atom. It was confirmed by fragmentation of *m/z* 384 producing a signal at *m/z* 305, due to the loss of the bromine atom. NMR analysis, including ^{1}HNMR spectrum in deuterated methanol (CD_3OD) and the connectivity deduced by heteronuclear multiple bond coherence (HMBC) heterocorrelations, allowed the structural assignment, which was in agreement with the reported data for discorhabdin G isolated from *L. apicalis* [21].

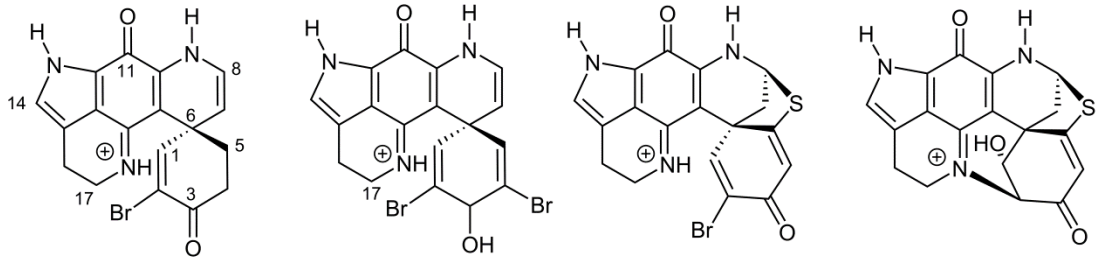

Fig. 1. Molecular structures of metabolites **1-4** isolated from the Antarctic sponge *Latrunculia* spp. as trifluoroacetate salts and tested for cholinesterase inhibition: discorhabdin G (**1**), 3-dihydro-7,8-dehydro discorhabdin C (**2**) discorhabdin B (**3**) and discorhabdin L (**4**).

The same three-step sequence was required for pure compound **2**, obtained evaporating the fraction eluted at 15.2 min in the last step of the work-up for the *L. biformis* extract by cyano HPLC preparative analysis. ESI-MS spectrum recorded in positive ion mode showed signals at: (i) *m/z* 462/464/466, corresponding to the M^+ ion and diagnostic for the presence of two bromine atoms, (ii) *m/z* 444/446/448, attributable to the $[M\text{-}H_2O]^+$ ion which supports the presence of a hydroxyl group in the structure and (iii) *m/z* 365/367, which are typical of the contribution of two bromine atoms and are due to the $[M\text{-}H_2O\text{-}Br]^+$ ion. NMR assignments, supported by long-range $^1H,^{13}C$ correlations by HMBC experiment, were in agreement with previous data reported for 3-dihydro-7,8-dehydro discorhabdin C [22].

The ^1H NMR spectrum of the crude methanol extract of *L. bocagei* showed a less complex mixture than that from *L. biformis*, with signals corresponding to two main compounds. These required only a two-step sequence of HPLC purification using a cyano stationary phase and elution with water/ methanol/ TFA 60:40:1 (v/v/v) to isolate discorhabdin B (**3**) and discorhabdin L (**4**) as trifluoroacetate, respectively (Fig. 1). They belong to the discorhabdin subclass that is structurally characterised by an additional sulfur bridge between the C-5 and C-8 positions.

(+)-Discorhabdin B was recovered by evaporation of the fraction eluted at the later retention time (15.8 min). The assignment that identified the structure of this monobrominated metabolite was supported by the isotopic cluster at *m/z* 414/416, corresponding to the M^+ ion. MS/MS fragmentation, carried out by direct infusion in methanol, indicated that the selected ion at *m/z* 414 gave signals at *m/z* 334 and *m/z* 302, which are attributable to the loss of HBr and HBr plus a S atom, respectively. The ^1H-NMR spectrum recorded in CD_3OD showed signals that were essentially superimposable on those previously reported for (+)-(6S, 8S)-discorhabdin B, first

isolated as its hydrochloride salt from an unclassified *Latrunculia* sp. collected along the New Zealand coast [23], and was characterised by comparison with discorhabdin A, which was established by X-ray diffractometry. The optical activity was also in agreement with that reported for a methanolic solution of (+)-discorhabdin B at a similar concentration. This measurement is particular, because also the enantiomeric (-)-discorhabdin B has been isolated in some cases [16].

(-)-Discorhabdin L (**4** in Fig.1) was recovered by evaporation of the fraction eluted at the earlier retention time (6.5 min) under the same chromatographic conditions for discorhabdin B. Its structural elucidation was obtained on the basis of the M^+ signal at *m/z* 352 in ESI-MS spectrum and by comparing the ^{1}H-NMR data with previously reported ones [24]. Some considerations relating to its optical activity are of note. Discorhabdins are pigments with visible absorbance that can encroach on the sodium line at 589 nm that is used for optical rotation measurements, so that different values at different concentrations can be obtained, with an $[\alpha]_D$ value of zero when a too high concentration is used. This behaviour was observed for discorhabdins bearing the additional ring through the connectivity between N(18) and C(2), as for discorhabdin L [25]. The (-)-(1S,2R,6S,8R) configuration that was earlier assigned for discorhabdin L through circular dichroism analysis was also in agreement with the isolation of the enantiomeric (+)-discorhabdin L [16].

The purity of the discorhabdins **1**-**4** used for the biological evaluation was verified by LC–ESI-MS analysis (Figs. S1-S4).

2.2. In vitro *AChE and BChE inhibitory activities*

Among the metabolites purified here, discorhabdin B (**3**) and 3-dihydro-7,8- dehydrodiscorhabdin C (**2**) were found to be the most cytotoxic against different murine and human tumour cell lines, with IC_{50} values around 0.1 μM [22, 26, 27]. Lam et al. [28] reported that discorhabdins that embody a ring closure between N-18 and C-2, such as discorhabdin L (**4**), have modest cytotoxic activity, with IC_{50} values from 1 μM to 15 μM [26, 27]. Discorhabdin G (**1**) was shown to have antibacterial activity and to cause feeding deterrence behaviour in the major Antarctic sponge predator *Perknaster fuscus* [21].

The cholinesterase inhibitory activities were here determined for the pure discorhabdins **1**-**4** against eeAChE, recombinant human AChE (hAChE), and horse serum BChE. Each of these metabolites effectively inhibited the cholinesterases in a dose-dependent manner (not shown). The

highest inhibitory activities were seen against eeAChE, which probably reflects the ecological role of these sponge metabolites in deterring possible predators. Discorhabdin G (**1)** and discorhabdin B (**3**) were the most potent AChE inhibitors of the series, with respective IC_{50} values of 1.3 µM and 5.7 µM towards eeAChE, and 116 µM and 49.5 µM towards hAChE (Table 1).

The inhibitory constants (K_i) corresponding to these two most potent AChE inhibitors, **1** and **3**, were 1.6 µM and 1.9 µM towards eeAChE, and 56.2 µM and 22.8 µM towards hAChE, respectively (Table 1). These IC_{50} and K_i values are within the pharmaceutically interesting regime when compared with commercial inhibitors used for the treatment of patients with Alzheimer's disease. Physostigmine was used as the positive control and it showed an IC_{50} of 3 µM towards eeAChE (Table 1), which is comparable to reported value [29], whereas its IC_{50} obtained for inhibition of hAChE (14.5 µM) was considerably higher than the IC_{50} reported for AChE isolated from human brain cortex (31 nM; [10]). As an additional reference, the IC_{50} of galantamine is in the range of 0.25-2.4 µM for eeAChE, and 1.07 -8.7 µM for hAChE [29].

For the inhibition of horse serum BChE, discorhabdin G (**1**) and 3-dihydro-7,8-dehydro discorhabdin C (**2)** showed the strongest inhibition among the tested compounds, with IC_{50} of 7 µM and 15.8 µM, respectively (Table 1). In comparison, the IC_{50} of the reference compound physostigmine salicylate was 28.5 µM (Table 1), while galantamine (1 mM) was reported to inhibit the BChE activity by 80.3% [30, 31]. Discorhabdin G and 3-dihydro-7,8-dehydro discorhabdin C also showed low K_i, at 5.0 µM and 17.5 µM, respectively (Table 1).

The kinetics of the inhibition of these cholinesterases by the tested metabolites, and their analysis using Dixon plots further revealed that discorhabdins **1-3** act as reversible, competitive inhibitors through their binding to the active site of the free AChE or BChE (Fig. 2).

Table 1. Inhibition of electric eel acetylcholinesterase (eeAChE), human recombinant acetylcholinesterase (hAChE) and equine serum butyrylcholinesterase (BChE) by discorhabdin G (**1**), 3-dihydro-7,8-dehydrodiscorhabdin C (**2**), discorhabdin B (**3**) and discorhabdin L (**4**).

	eeAChE		**hAChE**		**BChE**	
Compound[a]	**IC_{50} (μM)**	**K_i (μM)**	**IC_{50} (μM)**	**K_i (μM)**	**IC_{50} (μM)**	**K_i (μM)**
1	1.3±0.2	1.6	116±9	56.2	7.0±1.0	5.0
2	14.5±1.5	3.5	152±12	98	15.8±3.5	17.5
3	5.7±0.8	1.9	49.4±7.5	22.8	137±14.5	76
4	25.7±3.0	15.0	158±15	n.d.	531±45.0	n.d.
Physostigmine	3.0±0.3		14.5±2.0		28.5±3.0	

[a]Discorhabdin as trifluoroacetate (TFA) salt, physostigmine as salicylate salt.
n.d. not determined due to lack of the substance

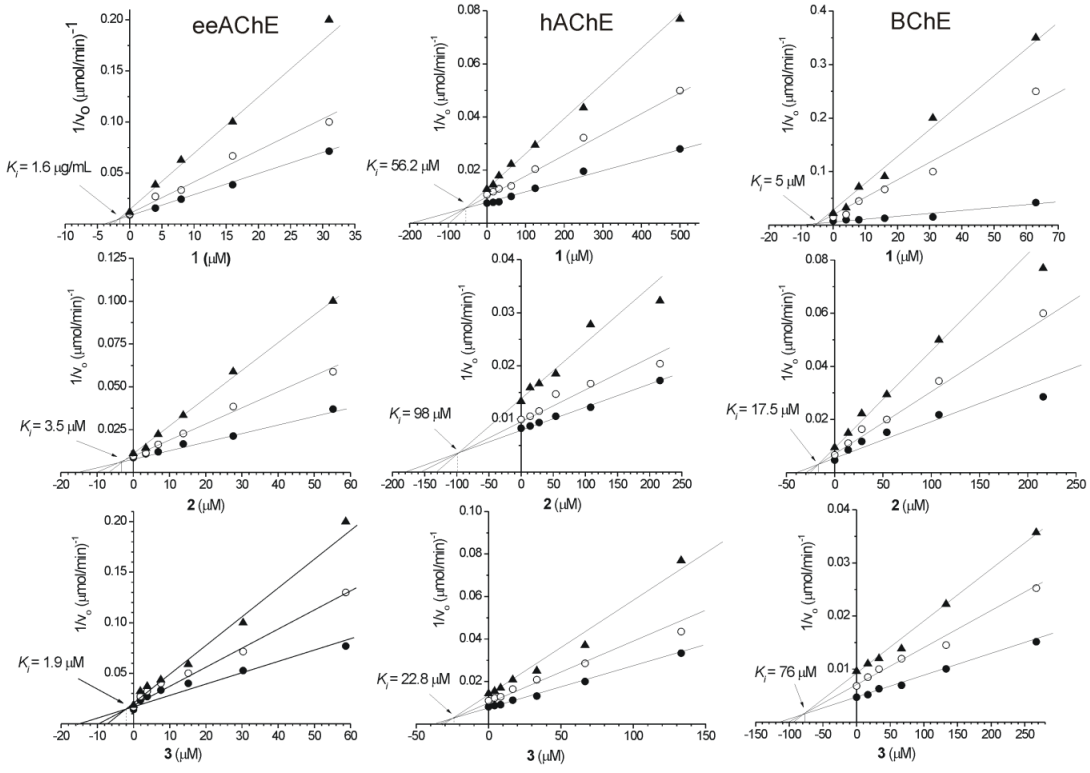

Fig.2. Determination of type of inhibition and inhibition constants (K_i) for discorhabdin G (**1**), 3-dihydro-7,8-dehydro discorhabdin C (**2**) and discorhabdin B (**3**) towards electric eel acetylcholinesterase (eeAChE; left panels), human recombinant acetylcholinesterase (hAChE; middle panels), and horse serum butyrylcholinesterase (BChE; right panels) by Dixon plot analysis. The concentrations of the substrate acetylthiocholine were 0.25 mM (full triangles), 0.5 mM (open circles) and 1 mM (full circles).

2.3. Molecular docking

In order to understand the interactions of the discorhabdins with the active sites of AChE enzymes and to propose a plausible binding mode that can explain the observed inhibitory activities, docking calculations were carried out using the AutoDock programme. Data for ee AChE (1C2O) are available by X-ray analysis with a too low resolution (4.2 Å) to be used in docking calculation, so that *Tetronarce californica* (1DX6, 2.3 Å resolution) was adopted as model system.

Preliminary comparison between these two structures was possible using the TM align algorithm, which obtained 59.5% equivalence in amino acid sequence, and very good overlap of their secondary structures. Mostly, these two AChEs showed the same amino acid residues in the active sites, except for phenylalanyl unit F330 in *T. californica* AChE that was replaced by tyrosine Y330 in eeAChE, which indicated very similar active sites for the two AChEs (Fig. S5).

The calculations were performed by Autodock Vina, adopting grid boxes with a spacing of 1.00 Å (details in Materials). The lacking of 3D structure for horse BuChE prevented a similar computational approach.

The docking results for *T. californica* AChE with the tested discorhabdins indicated a behaviour in line with the experimental data. Here, discorhabdin G (**1**) showed the lowest value of energy and the highest number of hydrophobic interactions, although with no specific H-bonds, which is in agreement with the highest observed inhibitory activity. The experimental trend of **1**>**3**>**2**>**4** is supported by the computational data that take into account the energy, the hydrogen bonds and their distances, and the numbers of hydrophobic interactions (Table 2).

Table 2. Data from docking calculation of discorhabdins **1**-**4** with the indicated AChEs.

Compound[a]	*Tetronarce californica* AChE (1DX6)			*Homo sapiens* AChE (4MOE)		
	ΔE[b]	**H-bond[c,d]**	**Aminoacidic hydrophobic interactions**	**ΔE[b]**	**H-bond[c,d]**	**Aminoacidic hydrophobic interactions**
1	-12.0	-	D72,W84,G117, G118, Y121,S122, G123,Y130, E199, F330,F331, Y334, H440	-10.1	-	Y72, D74, Y124, W286, L289,Q292, S293, V294, F295, Y341
1a	-11.5	N13-Y130 (2.83)	D72,W84,G117, G118, Y121,S122, G123, E199, F330, F331, Y334, H440	-10.2	N13-Y124 (2.99)	Y72, D74, W286, L289, Q292, S293, V294, F295, Y341
1 enol form	-11.2	-	W84,G117, G118, Y121, S122, G123, Y130, E199, F330, F331, Y334, H440	-9.8	-	Y72, D74, Y124, W286, L289, Q292, S293, V294, F295, Y341
1a enol form	-10.9	N13-Y130 (2.84)	W84,G117, G118, Y121, S122, G123, E199, F330, F331, Y334, H440	-9.9	N13-Y124 (2.89)	Y72, D74, W286, L289, Q292, S293, V294, F295, Y341
2	-10.6	HO3-D72 (3.31) N9-W84 (3.16)	S81,G117, G118, Y121, S122, G123, Y130, E199, F330, Y334, H440	-10.0	N9-Y72 (3.02)	Y124, W286, L289, Q292, S293, V294, F295, Y341
2a	-10.6	N9-E199 (3.23) N13-Y130 (2.87)	W84,G117, G118, Y121, S122, S124, G123, L127, Y130, E199, F290, F330, F331, Y334, H440	-9.8	N9-Y72 (2.89) N13-Y124 (3.11)	W286, L289, Q292, S293, V294, F295, Y341
3	-11.7	C3=O-G118 (3.15) C3=O-G119 (3.17) C3=O-S200 (3.17)	D72,W84, Y121, S122, G123,Y130, F330, F331, H440	-9.3	N9-Y72 (2.87) C11=O-Y72 (3.30) N13-Y124 (3.18)	W286, S293, V294, F295, Y341
3a	-11.7	C3=O-G118 (3.13) C3=O-G119 (3.18) C3=O-S200 (3.20)	D72,W84, Y121, S122,G123,Y130, F330, F331, H440	-9.1	N9-Y72 (2.80) C11=O-Y72 (3.34) N13-Y124 (3.06)	D74, W286, S293, V294, F295, Y341
4	-11.6	C3=O-S200 (2.85)	W84,G117, G118, Y121,S122,G123, Y130, F330,F331, H440	-9.2	N9-S293 (2.83)	D74, Y124, W286, V294, F295, Y341
4 enol form	-11.1	C3=O-S200 (2.85) N13-W84 (3.09)	G117, G118,Y121, S122, G123,Y130, F330, F331, H440	-9.2	C3=O-Y72 (2.93) N9-S293 (2.82)	D74, Y74, W286, V294, Y341
Physostigmine	-8.0	C(O)NH-Y130 (3.08)	D72, W84, G117, G118 Y121,S122, E199, S200, F330, F331, Y334, H440	-7.7	-	Y72, Y124,W286, S293, V294, F295, F297, F338

[a] **1a**, **2a** and **3a** as deprotonated form; [b] Calculated docking energy in Kcal/mol; [c] Numbering for discorhabdin structures as reported in Fig.1; [d] H-bond distance in Å are reported in brackets.

The docking results for each of the tested discorhabdins with hAChE showed lower energy and fewer hydrophobic interactions when compared with inhibition of *T. californica* AChE, which is in line with the experimental behaviour of inhibition towards eeAChE and hAChE tested here. For the discorhabdin G complex with hAChE, the computational data showed lower stability (i.e., corresponding to less negative energy), fewer hydrophobic interactions and a lack of H-bonds, compared to the discorhabdin G complex with *T. californica* AChE. These computational results support the lower inhibition achieved by discorhabdin G with hAChE than with *T. californica* AChE.

These results were in line with the experimental data that showed the trend of discorhabdins **3** > **1** > **2** ~ **4**. As the most active of this series, discorhabdin B (**3**) is supported by its three relevant H-bonds, in addition to a series of hydrophobic interactions. A visualisation of ligands **1-4** in the active sites of AChEs from the molecular study is reported in Figs. 3, 4 and S6. It is notable that tryptophan W286, valine V294, tyrosine Y341, and phenylalanine F295 are the amino acid residues of hAChE that are involved in each of these complexes between hAChE and discorhabdins.

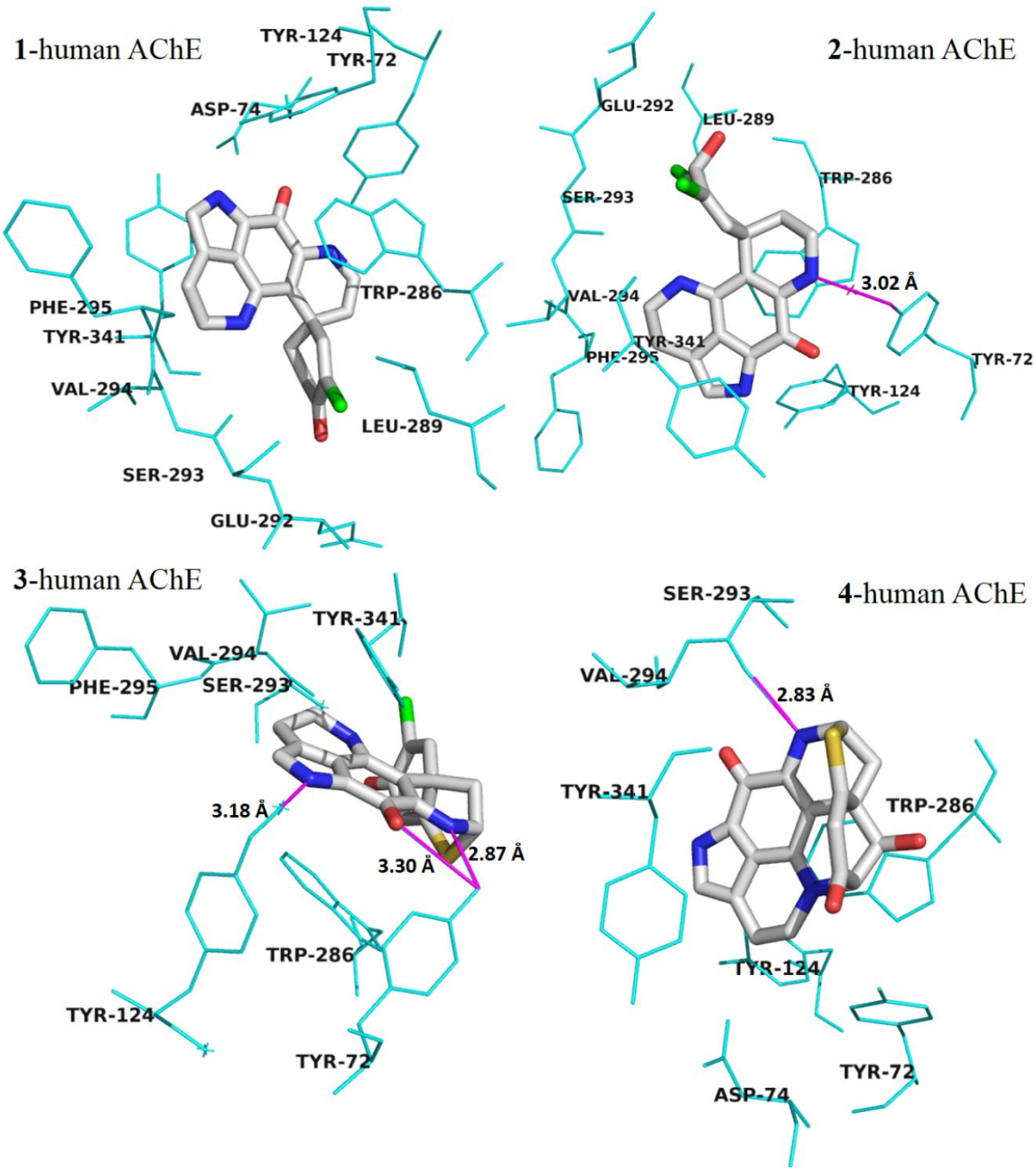

Fig. 3. Three-dimensional representations for the interactions of discorhabdin G (**1**), 3-dihydro-7,8-dehydro discorhabdin C (**2**), discorhabdin B (**3**) and discorhabdin L (**4**) with the electric ray (*T. californica*) AChE (left) and human *Homo sapiens* AChE (right) according to the docking calculations, with indications of H-bonds.

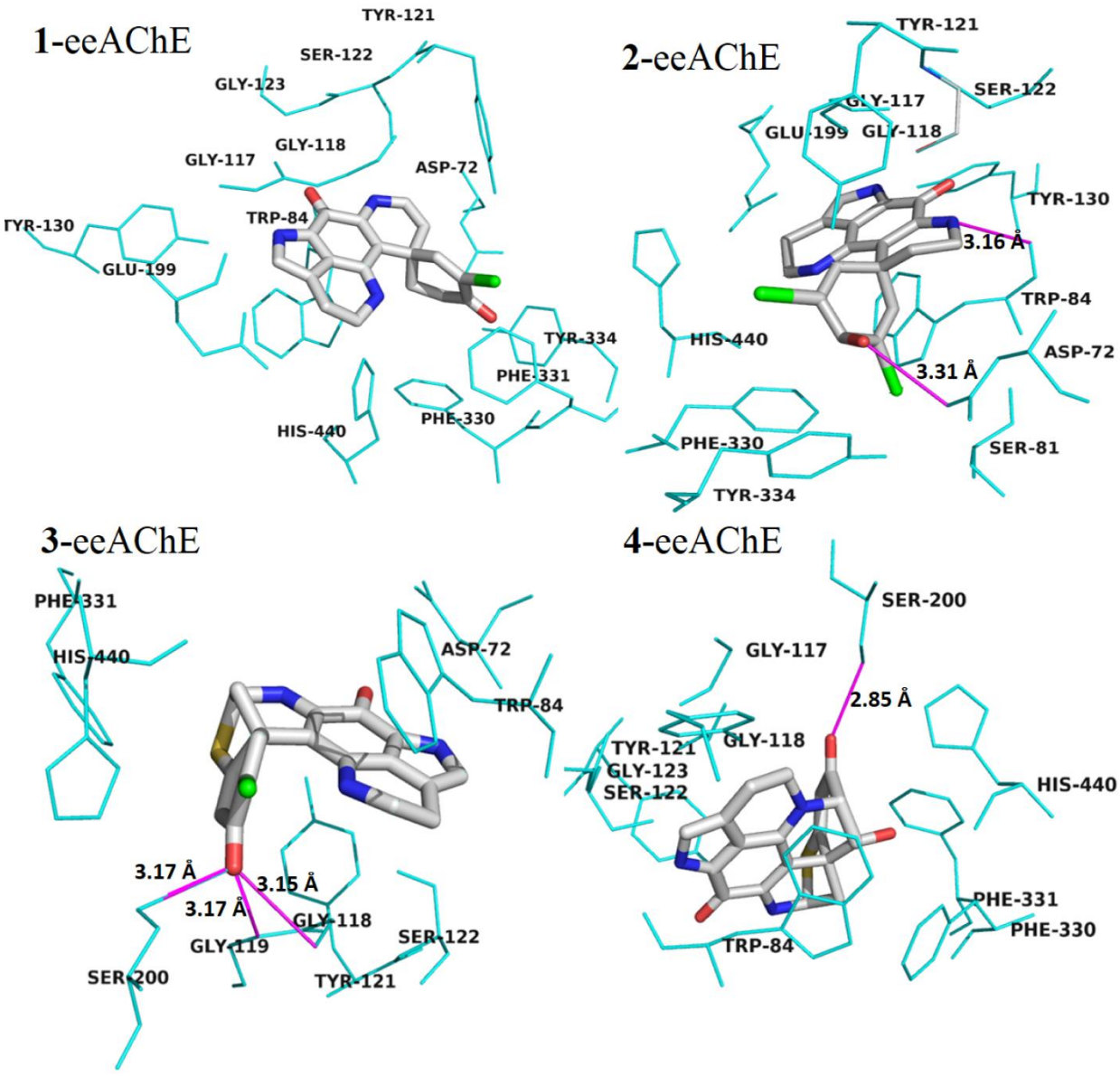

Fig. 4. Three-dimensional representations for the interactions of discorhabdin G (**1**), 3-dihydro-7,8-dehydro discorhabdin C (**2**), discorhabdin B (**3**) and discorhabdin L (**4**) with the electric ray (*T. californica*) AChE according to the docking calculations, with indications of H-bonds.

For discorhabdins G and L the enolic forms corresponding to the keto groups at the C-3 position are possible through a keto-enolic equilibrium, although their contributions were not evident in the NMR analysis. However, these enolic tautomers were taken into account in the docking calculations, and they demonstrated similar results to the corresponding keto forms. The computational analysis also involved the deprotonated forms of discorhabdins G and B, and 3-dihydro-7,8-dehydro discorhabdin C, as their free imines (**1a-3a** in Table 2), although these showed no effective changes in comparison with their protonated forms **1-3**. This was expected, because

N18 position is not involved in any of the interactions of discorhabdins **1**-**4**, and also because at the physiological pH used in the experimental assays, they would have been in their protonated forms. In addition, support comes from the observation that the crude methanol extract of *L. biformis* showed the same inhibitory activity on eeAChE as its protonated form that was obtained after treatment with the same water/methanol /TFA eluent used in the chromatographic isolation (IC_{50} = 1.6 µg dried extract/ mL).

Taking into account the interactions with hAChE that are more relevant for further biological applications, a qualitative correlation between structures and bioactivities indicated that the HN9/ OC11/ HN13 moiety is involved in H-bonds for the most active discorhabdin B, as well as for the other metabolites, although through hydrophobic interactions. This result can be used for the development of synthetic analogues with simpler structures.

2.4. Electrophysiological study of discorhabdin G

The use of AChE inhibitors can produce unwanted side effects, like single twitch potentiation in muscle, and the inability of skeletal muscle to sustain tetanic contraction [32-34]. Therefore, additional electrophysiological investigations were carried out with one of the most active of these discorhabdins, discorhabdin G. These were designed to determine its effects on nerve-evoked and directly elicited single muscle twitches and on tetanic contractions of the isolated mouse hemidiaphragm with the corresponding nerve.

While 8.43 µM discorhabdin G reduced the eeAChE activity *in vitro* by 80%, it appeared to have no effects on directly and indirectly evoked muscle twitch amplitudes, nor on the amplitudes of directly and indirectly evoked tetanic muscle contraction (Figs. 5, S7 and S8).

Inhibition of the AChE of the neuromuscular junction is associated with the inability to sustain a tetanic contraction under repetitive high frequency stimulation of the motor nerve [35]. The effects of discorhabdin G on the maximal amplitude of nerve-evoked sustained contraction was thus also investigated. There were no observable effects of discorhabdin G on the indirectly evoked tetanic contraction (Fig. 5).

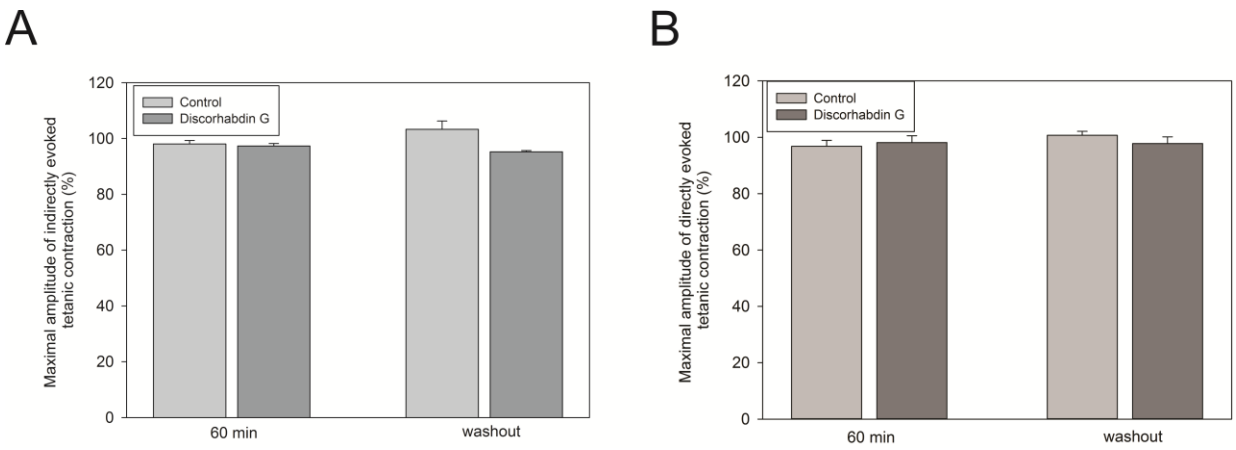

Figure 5. Effects of 8.43 µM discorhabdin G on nerve evoked (A) and directly elicited tetanic (B) contractions in the isolated mouse hemidiaphragm preparation, with 60 min of treatment and following washout. Data are means ±SEM (n = 3). Discorhabdin G *versus* control: *P* >0.05 in all cases (two-tailed Student t-tests).

To determine possible inhibitory effects on AChE in the neuromuscular junction, electrophysiological recordings from superficial muscle fibres were performed in the same neuromuscular preparation exposed to 2 µM conotoxin GIIIB, which effectively blocks NaV1.4 sodium channels in vertebrate skeletal muscle, to thus prevent muscle fibre contraction. Discorhabdin G did not increase the amplitude of the EPPs or the EPP half decay after either 30 min or 60 min exposure of the neuromuscular preparation to this discorhabdin (Fig. 6).

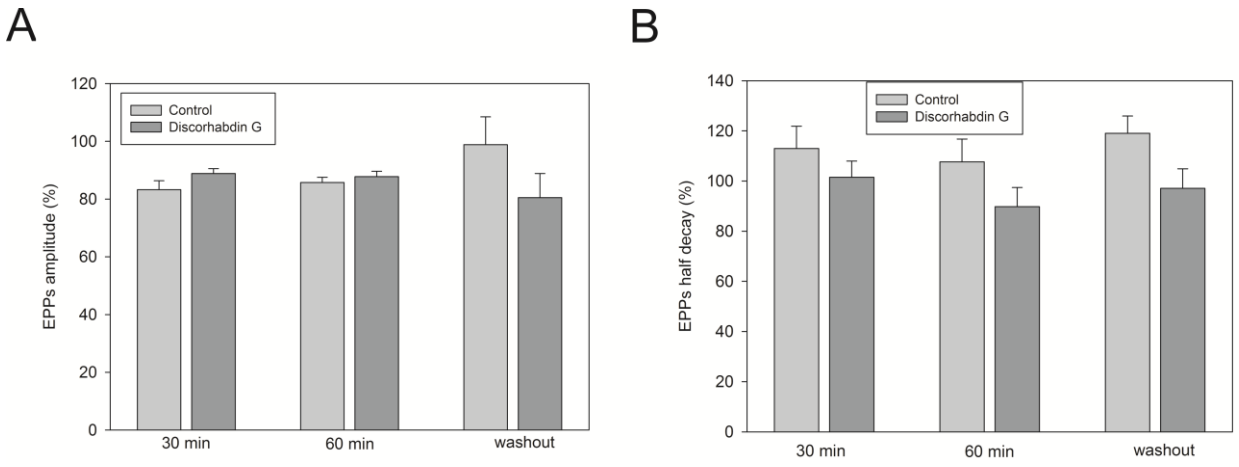

Figure 6. Effects of discorhabdin G on EPP amplitudes (A) and EPP half decay (B). Mouse hemidiaphragm preparations were pretreated for 30 min with 2 µM conotoxin GIIIB, and all experiments were performed in the presence of 2 µM conotoxin GIIIB to record full sized EPPs and to prevent muscle twitches. Data are means ±SEM, from 8-12 muscle fibres from two or three different nerve muscle preparations. Discorhabdin G *versus* control: *P* >0.05 in all cases (two-tailed Student t-tests).

3. Conclusions

For many years, the *Latrunculia* spp. sponges have been the focus of studies, as they represent a source of a wide series of discorhabdin alkaloids that show interesting cytotoxic, antimalarial, antimicrobial and anti-inflammatory activities. To date, cholinesterase inhibitory activities have been assigned only to crude extracts from some species of tropical and Antarctic *Latrunculia* spp. sponges, without associating them to any identified pure metabolites in these extracts. Based on the data reported here, these discorhabdin metabolites appear to be responsible for the previously described cholinesterase inhibitory activities of such extracts. The evaluation of isolated discorhabdins G (**1**), B (**3**) and L (**4**), and 3-dihydro-7,8-dehydro discorhabdin C (**2**) against both eeAChE and hAChE, and also horse serum BChE, demonstrated a competitive reversible mechanism of inhibition with discorhabdin G as the most potent inhibitor of eeAChE and horse serum BChE, and discorhabdin B as the most potent inhibitor of hAChE. Docking calculations for different AChEs defined the interactions involved between these discorhabdin ligands and the active sites of the AChEs, which provided further support for the experimental data. Electrophysiological experiments with discorhabdin G showed that it has no undesirable effects on neuromuscular transmission and skeletal muscle function in this setting, thus favouring its use in the therapy of cholinesterase inhibition, as this appears to avoid the side effects produced by some of the known cholinesterase inhibitors. Thus, based on the scaffold of discorhabdin metabolites, these findings are promising as a guide towards the synthesis of potential agents for the treatment of Alzheimer's disease.

4. Materials and Methods

4.1. Chemistry

All of the solvents used were from Riedel-de Haën–Sigma Chemical Co., and were of HPLC grade. Evaporation was carried out at 25 °C and reduced pressure. Thin layer chromatography was carried out on Merck RP-18 F_{254}, Merck CN F_{254} or Kieselgel 60 0.2-mm plates, with visualisation using UV light or marking of visible spots. NMR spectra were recorded on a spectrometer Bruker-Avance 400 using a double-resonance broadband inverse (BBI) probe for ^{1}H at 400 MHz and a broadband observe (BBO) probe for ^{13}C at 100 MHz in CD_3OD, relative to the solvent residual signals, with δ_H = 3.31 ppm and δ_C = 49.00 ppm, respectively. Structural assignments were

supported by HMBC experiments comparison with reported data. Polarimetric data were obtained with an apparatus (Jasco-DP-181) equipped with a sodium lamp at 589 nm (line D) or a mercury lamp at 577 nm, with $[\alpha]_D$ reported as dm^{-1} deg mL g^{-1}. Infrared spectra were recorded using a spectrometer (FT-IR Tensor 27; Bruker) equipped with an attenuated transmitter reflection device at 1 cm^{-1} resolution in the absorption region 4,000 cm^{-1} to 1,000 cm^{-1}. A thin solid layer was obtained by evaporation of the methanolic solution of the samples. The instrument was purged with a constant dry nitrogen flow. Spectra processing was carried out with the Opus software package. ESI-MS mass spectra were recorded using a Bruker Esquire-LC spectrometer equipped with an ion trap analyser. The atmospheric pressure electrospray ion source was used in positive ion mode, under the following conditions: source temperature, 300 °C; drying gas, N_2; flow rate, 4 L/min; and scan range, 100-1,000 *m/z*. The mass spectra were analysed using Data Analysis, version 3.0 (Bruker Daltonics GmbH). Online liquid chromatography–ESI MS analysis was performed using liquid chromatograph (Hewlett-Packard) with a photo diode array detector (1100 Series Agilent). The HPLC conditions included: Lichrospher 100 CN column (250 mm × 4 mm; 5 μm); flow rate, 1 mL/min; detector, 254 nm; gradient mobile phase, water/ methanol/ TFA, from 80:20:1 (v/v/v) to 50:50:1 (v/v/v), over 20 min, and then to 0:100:1 (v/v/v) over 30 min.

4.2. Sponge collection

Two specimens of cold-water sponges that belong to the genus *Latrunculia* were obtained from the Senckenberg Research Institute and Natural History Museum, Germany. These sponges had been dredged from coastal shelf environments around the Antarctic Peninsula (60°-70° S; 8°-61° W) during the deployment of an Agassiz trawl, at depths between 200 m and 600 m, during the ANT XXIX/3 expedition of the German Research Vessel "*Polarstern*" in 2013 (for environmental and faunistic information, see [36]). The sponge samples were frozen at −20 °C immediately after collection, and lyophilised prior to extraction. One specimen (SMF11203) was collected at 330 m in depth and was identified as *Latrunculia biformis*, and the other specimen (SMF11172) was collected at 430 m in depth and was identified as *Latrunculia bocagei*. The sponge samples have been entered in the Senckenberg Sammlungs management database (http://sesam.senckenberg.de/).

4.3. Isolation and structural characterisation of discorhabdin alkaloids 1-4

For each sponge specimen, 0.5 g freeze-dried sponge material was extracted ultrasonically (3×) using methanol, for 1 h at 25 °C. After each extraction step, the mixture was centrifuged to remove solid particles, and then the extract was collected and evaporated to dryness on a rotatory vacuum evaporator at 25 °C. These extracts were dark brown in colour, and constituted the crude organic extracts (*L. biformis*: sample v171, 180 mg; *L. bocagei*: sample v105, 157.9 mg).

The methanol extract from *L. biformis* was dissolved in water/ methanol and subjected to HPLC purification on a preparative CN column (Merck Lichrospher 100, 250 mm × 4.0 mm, 5 μm) eluting with water/ methanol/ TFA (60:40;1 v/v/v), at a flow rate of 5 mL/min and under UV detection at 254 nm. The fraction collected at 7 min was evaporated and injected again onto an RP-18 HPLC column (Merck Lichrosphere) and eluted with acetonitrile/ water/ TFA 30:70: 1 (v/v/v). The fraction that eluted at 11 min was evaporated, resuspended in acetonitrile/ water and injected onto the previously used CN column, eluting with acetonitrile/ water/ TFA 30:70:1 (v/v/v). The fraction collected at 6.5 min was concentrated to give pure discorhabdin G trifluoroacetate salt (**1**, 3.1 mg). The fraction eluted at 15.2 min was evaporated to give pure trifluoroacetate salt of 3-dihydro-7,8-dehydrodiscorhabdin C (**2** in Fig.1, 4.5 mg).

The methanol extract from *L. bocagei* was subjected to preparative HPLC under the same conditions as the first step adopted for purification of discorhabdins **1** and **2**. The fraction collected at 6.5 min was evaporated to dryness and the residue was further purified on the same column, by elution with water/ methanol/ TFA 60:40:1 (v/v/v) The peak obtained at 15.8 min gave (+)-discorhabdin B trifluoroacetate salt (**3** in Fig. 1, 3.2 mg, 0.002% in the crude extract). The fraction collected at 4.2 min in the first HPLC step gave a residue which was injected onto the same column, eluting with water/ methanol/ TFA 60:40:1 (v/v/v), to obtain (-)-discorhabdin L trifluoroacetate salt (**4**) from the fraction eluted at 7.0 min (1.9 mg, 0.0012% in the crude extract).

*4.3.1. Data for (+)discorhabdin G (**1**)*

Isolated as trifluoroacetate salt (MW = 498.25 g/mol), $[\alpha]_D$ = +28° (c 1.3 mg/mL, MeOH).

^{1}HNMR (400 MHz, CD_3OD): δ 7.65 (1H, s, H-1), 7.16 (1H, s, H-14), 6.38 (1H, d, *J* = 7.8 Hz, H-8), 5.40 (1H, d, *J* = 7.8 Hz, H-7), 3.89 (2H, t, *J* = 7.8 Hz, 2H-17), 2.98 (3H, m, H-4a and 2H-16), 2.70-2.30 (series of m, H-4b, and 2H-5). ^{13}CNMR (100 MHz, CD_3OD, detectable signals): δ 189.9 (C3), 154.4 (C1), 146.2 (C10), 126.8 (C14), 125.0 (C2), 124.5 (C8), 120.7 (C15), 112.9 (C7), 98.7

(C20), 46.1 (C6), 45.9 (C17), 43.0 (C6), 36.6 (C5), 32.6 (C4), 19.8 (C16). ESI(+)MS *m/z* 384/386 $[M]^+$, ESI(+)MS/MS (384/386): *m/z* 305.

*4.3.2. Data for (-)-3-dihydro-7,8-dehydro-discorhabdin C (**2**)*

Isolated as trifluoroacetate salt (MW = 577.15 g/mol), $[\alpha]_D$ = -70° (c 2.5 mg/mL, MeOH). ^{1}HNMR (400 MHz, CD_3OD): δ 6.67 (2H, s, H-1, H-5), 6.36 (1H, d, *J* = 7.8 Hz, H-8), 7.17 (1H, broad s, H-14), 4.71 (1H, s, H-3), 4.73 (1H, d, *J* = 7.8 Hz, H-7), 3.86 (2H, t, *J* = 7.7 Hz, H-17), 2.94 (2H, t, *J* = 7.7 Hz, H-16). ^{13}CNMR (100 MHz, CD_3OD, detectable signals): δ 167.2 (C11), 163.8 (COO^-), 158.7(C19), 132.7 (C1 and C5), 126.0 (C14), 124.0 (C21 or C12), 122.5 (C12 or C21), 122.2 (C2 and C4), 121.8 (C8), 121.5 (C15), 112.3 (C7), 93.7 (C20), 69.7(C3), 43.3 (C17), 17.6 (C16). ESI(+)MS *m/z* 462/464/466 $[M]^+$, ESI(+)MS/MS (462/464/466): *m/z* 444/446/448; 365/367.

*4.3.3. Data for (+)-discorhabdin B (**3**)*

Isolated as trifluoroacetate salt (MW = 528.30 g/mol), dark green solid: $[\alpha]_D$ = +545° (c 1.1 mg/mL, MeOH), +400° (c = 0.17, MeOH), reported by Perry et al. [21]). ^{1}HNMR (400 MHz, CD_3OD): δ 7.85 (1H, s, H-1), 7.21 (1H, s, H-14), 6.26 (1H, s, H-4), 5.70 (1H, d, *J* = 3.5 Hz, H-8), 3.94 and 3.83 (2H, two m, 2H-17), 2.92 (2H, dd, *J* = 6.5, 9 Hz, 2H-16), 2.80 (1H, d, *J* = 11.6 Hz, 1H-7), 2.55 (1H, dd, *J* = 11.6, 3.5 Hz, 1H-7). ^{13}CNMR (100 MHz, CD_3OD, detectable signals): δ 171.4 C(1), 168.7 (C11), 144.8 (C1), 127.0(C14), 126.4 (C2), 119.0 (C4), 94.9 (C20), 59.3 (C8), 43.0 (C17), 40.2 (C7), 18.2 (C16); from HMBC correlations: δ 153.7 (C19), 49.6 (C6). ESI(+)MS *m/z* 414/416 $[M]^+$, 436/438 $[M-H+Na]^+$; ESI(+)MS/MS (414/416): *m/z* 334, 302.

*4.3.4. Data for (-)-discorhabdin L (**4**)*

Isolated as trifluoroacetate salt (MW = 465.40 g/mol), dark-green solid: $[\alpha]_{577}$ = -407° (c 0.8 g/mL, MeOH). ^{1}HNMR (400 MHz, CD_3OD): δ 7.11 (1H, s, H-14), 6.14 (1H, s, H-4), 5.58 (1H, brd, *J* = 3.6 Hz, H-8), 4.63 (1H, d, *J* = 3.6 Hz, H-1), 4.15 (d, *J* = 3.6 Hz, H-2), 4.01 (1H, ddd, *J* = 14.2, 7.5, 3.0 Hz, 1H-17), 3.90 (1H, ddd, *J* = 14.2, 7.5, 3.0 Hz, 1H-17), 3.18 and 3.06 (2H, two m, 2H-16), 2.95 (1H, dd, *J* = 12.0, 3.6 Hz, 1H-7), 2.57 (1H, d, *J* = 12.0 Hz, 1H-7). ^{13}CNMR (100 MHz, CD_3OD): δ 167.2(C11), 148.4 (C10), 127.0 (C14), 118.9 (C15), 114.1(C4), 102.0 (C20), 68.5(C1 or C2), 67.8 (C2 or C1), 63.7 (C8), 51.5 (C17), 37.9 (C7), 20.1 (C16); from HMBC correlations: δ 184.7 (C3), 171.4 (C5), 125.6 (C12). ESI(+)MS *m/z* 352 $[M]^+$, ESI(+)MS/MS (352): *m/z* 335, 324, 281, 250.

4.3.5. Protonation of methanol extract from Latrunculia biformis

The residue from crude methanol extract (5 mg) was suspended in 1 mL of methanol/ water/ TFA as used for the HPLC purification of discorhabdin metabolites. This solution was stirred at room temperature for 15 min, and then evaporated to dryness, to give the residue used in the further biological assays.

4.4. Cholinesterase inhibition

The cholinesterase activities were measured by the Ellman method [37], using acetylthiocholine chloride (0.25, 0.5 or 1.0 mM; Sigma, USA) as substrate in 100 mM potassium phosphate buffer, pH 7.4, at 25 °C. Three cholinesterases were used as the source of enzyme, at the final concentration of 0.0075 U/mL: eeAChE (from *Electrophorus electricus*), hAChE, and horse serum BChE (all Sigma, USA). The hydrolysis of acetylthiocholine chloride was followed in a microplate reader (Kinetic; Dynex Technologies, USA) at 405 nm. Stock solutions of the discorhabdins (2 mg/mL) were prepared in ethanol/ deionised water (1:9; v/v). Cholinesterase inhibition was monitored over 5 min from the addition of the discorhabdins (progressively diluted in 100 mM potassium phosphate buffer, pH 7.4). Physostigmine salicilate (Sigma, USA) was dissolved in 100% ethanol and used as the positive control. All readings were corrected according to the appropriate blanks. Blank reactions without the inhibitors were run in the presence of the appropriate ethanol/ water dilutions (1:9; v/v) for the discorhabdins, or in the presence of pure ethanol for physostigmine. Each measurement was repeated at least three times. The inhibitory constants (K_i) for discorhabdin L towards hAChE and horse serum BChE were not determined, due to lack of the isolated discorhabdin L.

4.5. Muscle contraction

Male Balb/c mice (2-3 months old) were obtained from the Animal Breeding Facility in the Veterinary Faculty, University of Ljubljana. The study on isolated neuromuscular preparations was carried out in strict accordance with Slovenian legislation, as harmonised with the European Communities Council Guidelines (Directive 86/609/EGS of 24 November, 1986; Directive 2010/63/EU of 22 September, 2010). All *in-vitro* experiments on isolated organs were approved by the Administration of the Republic of Slovenia for Food Safety, Veterinary and Plant Protection

(permit no. 34401-12/2012/2). The mice were sacrificed by cervical dislocation, followed by immediate exsanguination. The diaphragm with corresponding phrenic nerves was dissected out and used. A hemidiaphragm was tightly pinned to the Rhodorsil-coated organ bath containing oxygenated standard Krebs-Ringer solution (154 mM NaCl, 2 mM $CaCl_2$, 5 mM KCl, 1 mM $MgCl_2$, 5 mM HEPES, 11 mM D-glucose, pH 7.4), at 22 °C to 24 °C. The tendinous side of the hemidiaphragm was attached with a steel hook *via* silk thread to an isometric force displacement transducer (FT 03; Grass Instruments, West Warwick, RI, USA). Before the beginning of the experiments, each hemidiaphragm preparation was left to equilibrate for 20 min, to achieve stable resting tension.

Nerve-evoked single isometric twitches were recorded as follows: the motor nerve of the isolated neuromuscular preparation was stimulated with a square-pulse stimulator (S-48; Grass Instruments, West Warwick, RI, USA) *via* a suction electrode, with pulses of 0.1 ms duration, 0.1 Hz stimulation rate, and supramaximal voltage typically 6 V to 8 V. Directly evoked single isometric twitches were evoked by stimulating the hemidiaphragm preparation with a platinum electrode assembly placed along the organ bath, with pulses of 0.1 ms duration, 0.1 Hz stimulation rate, and supramaximal voltage of 60 V to 80 V. Direct or nerve-evoked tetanic muscle contraction recordings were obtained by stimulating the hemidiaphragm with trains of pulses (1000 ms duration, at 80 Hz). The electrical signals from muscle contraction experiments were amplified using a strain gage amplifier (P122; Grass Instruments, West Warwick, RI, USA), and then digitised at a sampling rate of 1 kHz using a data acquisition system (Digidata 1440A; Molecular Devices, Sunnyvale, CA, USA). The effects of discorhabdin G on the muscle contraction of the hemidiaphragm preparation were measured over 60 min of exposure.

4.5.1. Muscle fibre membrane potentials

For the muscle fibre membrane potentials, the experiments were performed at room temperature (22-24 °C) on the mouse oxygenated hemidiaphragm preparations, pretreated for 30 min with 2 µM µ-conotoxin GIIIB, an inhibitor of muscle sodium channels, to prevent muscle contraction and to record full-sized endplate potentials. The resting membrane potential, endplate potentials (EPPs) and miniature endplate potentials (MEPPs) were recorded from endplate regions in superficial muscle fibres using intracellular borosilicate microelectrodes pulled with a microelectrode puller (P-97 Flaming/ Brown; Sutter Instruments, Novato, CA, USA) and filled with 3 M KCl.

Microelectrodes with resistance from 10 MΩ to 20 MΩ were used. The potentials were recorded before and 30 and 60 min after application of discorhabdin G, and 10 min after washing out discorhabdin G. The EPPs were evoked by stimulating the phrenic nerve with supramaximal square pulses (8-12 V) of 0.1 ms duration, 1 Hz stimulation rate. The EPP and MEPP recordings were digitised (Digidata 1440A), with the pClamp 10 software used. Data were analysed using the pClamp-Clampfit 10.2 programme. The amplitudes of EPPs were normalised to a membrane potential of -70 mV using Equation (1):

$$V_c = V_0 \times (-70) / E \quad (1),$$

where V_c is the normalised amplitude of the EPPs or MEPPs, V_0 is the recorded amplitude, and E is the resting membrane potential.

4.5.2. Data analysis and statistics

The statistical analysis of the data was carried out using SigmaPlot for Windows 12.5 (Systat Software Inc., Germany). The data are presented as means ±SEM. They were first tested for normality (Shapiro–Wilk) and equal variance for assignment to parametric or non-parametric analysis. For the membrane potential data, two-tailed Student t-tests were used, and $P \leq 0.05$ was considered to be statistically significant.

4.6. Computational details

Calculations were carried out on a PC running at 3.4 GHz on an Intel i7 2600 quad core processor with 8 GB RAM and 1 TB hard disk, with Windows 7 Home Premium 64-bit SP1 as the operating system. The ligands were build using PC Model version 6.0 (Serena Software, Bloomington, IN 47402-3076) and minimised using the force field MMX. The minimised molecules were saved in pdb extension. The AutoDock Tools (ADT) package version 1.5.6rc3 [38] was used to generate the docking input files and to analyse the docking results, with Autodock Vina 1.1.2 [39] used for the docking calculations. The different crystallographic structures of AChE were from the Protein Data Bank (PDB; http://www.pdb.org/). The structure of hAChE in complex with dihydrotanshinone (4MOE) and the structure of the *Tetronarce* AChE complexed with (-)-galantamine (1DX6) were determined by X-ray crystallography, with a resolution of 2.0 Å and 2.3 Å, respectively [40,41]. The structures were modified as follows: the ligand and all of the crystallisation water molecules were removed, with the file saved in pdb extension. All hydrogen

atoms were added using AutoDock Tools (ADT), and the Gasteiger–Marsili charges were calculated, with the resulting file saved in pdbqt extension. Rotatable bonds were defined for each minimised ligand molecule. For the docking calculation, for 4MOE, a grid box of 14 × 14 × 14 Å in the x, y and z directions was created, with spacing of 1.00 Å and centred at x = -17.171, y = -42.504, z = 25.612, and for 1DX6, a grid box of 16 × 16 × 16 Å in the x, y and z directions was created, with spacing of 1.00 Å and centred at x = 3.627, y = 64.986, z = 64.364. Vina parameters were set as follows: exhaustiveness of the local search, 100; number of conformations to calculate, 10. To validate the goodness of the calculation, the original ligand was re-docked and visual inspection of the data showed very tight overlap. The results are expressed as the energy associated to each ligand–enzyme complex in terms of the Gibbs free energy values. The visual ligand–enzyme interactions were displayed using LigPlot [42].

The structural comparisons of AChE 1DX6 from *Tetronarce californica* used in the docking calculations with AChE used in the biological assays (eeAChE 1C2O) and *Homo sapiens* hAChE (4MOE) were obtained by applying the TM-align server (version 20160521) [43].

Author contributions

T.B. purified the natural products from the crude extracts and wrote the manuscript; A.D. carried out molecular docking studies; P.Z. purified natural products and carried out part of the enzyme inhibition experiments, M.C.Ž. and R.F. carried out the electrophysiological experiments and wrote the manuscript; D.J. and D.K. collected the sponges during an Antarctic expedition, identified them, and prepared the crude extracts; Ž.K. wrote the manuscript; I.M. supervised the chromatographic purification of the metabolites, characterised their structures, and wrote the manuscript; K.S. planned, supervised, and carried out part of enzyme inhibition experiments, and wrote the manuscript.

Conflict of interest

The authors declare that there are no conflicts of interest regarding this work.

Acknowledgments

The authors gratefully acknowledge the Slovenian Research Agency (Research Programmes P2-0046, P1-0207, P4-0053), BI-FR-PROTEUS/17-18-001 project, and ERASMUS STT. T. Botić

wishes to thank the members of the Laboratory of Bioorganic Chemistry, Department of Physics, of the University of Trento, for their help and support during her visit to their laboratory. Special thanks go to Adriano Sterni for the mass spectra acquisition and to Mario Rossi for technical guidance. Christopher Berrie is gratefully acknowledged for editing and appraisal of the manuscript. D. Janussen wishes to thank all of her colleagues who participated in and were working together during the Antarctic 2013 winter expedition, ANT XXIX/3. Our thanks also go to the Captain and crew of the *RV Polarstern*. Deutsche Forschungsgemeinschaft (DFG) is acknowledged for financial support of the Antarctic Porifera Research Project (JA 1063/17-1).

Appendix A. Supplementary data

Supplementary material related to this article can be found at…

References

[1] K. Ubhi, E. Masliah, Alzheimer's disease: recent advances and future perspectives, J. Alzheimer's Dis. 33 (2013) 185-194.

[2] M. Prince, A. Wimo, M. Guerchet, G.-C. Ali, Y.-T. Wu, M. Prina, World Alzheimer Report 2015, The Global Impact of Dementia. An Analysis of Prevalence, Incidence, Cost and Trends, A.s.D. International, London, 2015.

[3] R.M. Lane, M. Kivipelto, N.H. Greig, Acetylcholinesterase and its inhibition in Alzheimer disease, Clin. Neuropharmacol. 27 (2004) 141-149.

[4] M. Singh, M. Kaur, H. Kukreja, R. Chugh, O. Silakari, D. Singh, Acetylcholinesterase inhibitors as Alzheimer therapy: from nerve toxins to neuroprotection, Eur. J. Med. Chem. 70 (2013) 165-188.

[5] E. Giacobini, Cholinesterase inhibitors: new roles and therapeutic alternatives, Pharmacol. Res. 50 (2004) 433-440.

[6] H.O. Tayeb, H.D. Yang, B.H. Price, F.I. Tarazi, Pharmacotherapies for Alzheimer's disease: beyond cholinesterase inhibitors, Pharmacol. Ther. 134 (2012) 8-25.

[7] L. Pezzementi, A. Chatonnet, Evolution of cholinesterases in the animal kingdom, Chem. Biol. Interact. 187 (2010) 27-33.

[8] B. Li, J.A. Stribley, A. Ticu, W. Xie, L.M. Schopfer, P. Hammond, S. Brimijoin, S.H. Hinrichs, O. Lockridge, Abundant tissue butyrylcholinesterase and its possible function in the acetylcholinesterase knockout mouse, J. Neurochem. 75 (2000) 1320-1331.

[9] M. Heinrich, H. Lee Teoh, Galantamine from snowdrop--the development of a modern drug against Alzheimer's disease from local Caucasian knowledge, J. Ethnopharmacol. 92 (2004) 147-162.

[10] D.J. Triggle, J.M. Mitchell, R. Filler, The pharmacology of physostigmine, CNS Drug Reviews 4 (1998) 87-136.

[11] Q. Zhao, X.C. Tang, Effects of huperzine A on acetylcholinesterase isoforms *in vitro*: comparison with tacrine, donepezil, rivastigmine and physostigmine, Eur. J. Pharmacol. 455 (2002) 101-107.

[12] I.E. Orhan, Nature: a substantial source of auspicious substances with acetylcholinesterase inhibitory action, Curr. Neuropharmacol. 11 (2013) 379-387.

[13] G.-P. Hu, J. Yuan, L. Sun, Z.-G. She, J.-H. Wu, X.-J. Lan, X. Zhu, Y.-C. Lin, S.-P. Chen, Statistical research on marine natural products based on data obtained between 1985 and 2008, Mar. Drugs 9 (2011) 514-525.

[14] J.W. Blunt, B.R. Copp, R.A. Keyzers, M.H. Munro, M.R. Prinsep, Marine natural products, Nat. Prod. Rep. 31 (2014) 160-258.

[15] T. Samaai, M. Kelly, Family Latrunculiidae Topsent, 1922, in: J.N.A. Hooper, R.W.M. Van Soest, P. Willenz (Eds.) Systema Porifera: A Guide to the Classification of Sponges, Springer US, Boston, MA, 2002, pp. 708-719.

[16] J.-F. Hu, H. Fan, J. Xiong, S.-B. Wu, Discorhabdins and pyrroloiminoquinone-related alkaloids, Chem. Rev. 111 (2011) 5465-5491.

[17] S. Abbas, M. Kelly, J. Bowling, J. Sims, A. Waters, M. Hamann, Advancement into the Arctic region for bioactive sponge secondary metabolites, Mar. Drugs 9 (2011) 2423-2437.

[18] Y. Wada, H. Fujioka, Y. Kita, Synthesis of the marine pyrroloiminoquinone alkaloids, discorhabdins, Mar. Drugs 8 (2010) 1394-1416.

[19] I. Nèeman, L. Fishelson, Y. Kashman, Isolation of a new toxin from the sponge *Latrunculia magnifica* in the gulf of aqaba red sea, Mar. Biol. 30 (1975) 293-296.

[20] T. Turk, J. Ambrožič Avguštin, U. Batista, G. Strugar, R. Kosmina, S. Čivović, D. Janussen, S. Kauferstein, D. Mebs, K. Sepčić, Biological activities of ethanolic extracts from deep-sea Antarctic marine sponges, Mar. Drugs 11 (2013) 1126-1139.

[21] A.Yang, B.J.Baker, J.Grimwade, A.Leonard, J.B.Mc Clintock, Discorhabdin alkaloids from the Antarctic sponge *Latrunculia apicalis*. J. Nat. Prod. 58 (1995) 1596-1599.

[22] E.M. Antunes, D.R. Beukes, M. Kelly, T. Samaai, L.R. Barrows, K.M. Marshall, C. Sincich, M.T. Davies-Coleman, Cytotoxic pyrroloiminoquinones from four new species of South African Latrunculid sponges, J. Nat. Prod. 67 (2004) 1268-1276.

[23] N.B. Perry, J.W. Blunt, M.H.G. Munro, Cytotoxic pigments from New Zealand sponges of the genus *Latrunculia* : discorhabdins a, b and c, Tetrahedron 44 (1988) 1727-1734.

[24] F. Reyes, R. Martín, A. Rueda, R. Fernández, D. Montalvo, C. Gómez, J.M. Sánchez-Puelles, Discorhabdins I and L, cytotoxic alkaloids from the sponge *Latrunculia brevis*, J. Nat. Prod. 67 (2004) 463-465.

[25] M. El-Naggar, R.J. Capon, Discorhabdins revisited: Cytotoxic alkaloids from southern Australian marine sponges of the genera *Higginsia* and *Spongosorites*, J. Nat. Prod. 72 (2009) 460-464.

[26] G. Lang, A. Pinkert, J.W. Blunt, M.H. Munro, Discorhabdin W, the first dimeric discorhabdin, J. Nat. Prod. 68 (2005) 1796-1798.

[27] T. Grkovic, A.N. Pearce, M.H. Munro, J.W. Blunt, M.T. Davies-Coleman, B.R. Copp, Isolation and characterization of diastereomers of discorhabdins H and K and assignment of absolute configuration to discorhabdins D, N, Q, S, T, and U, J. Nat. Prod. 73 (2010) 1686-1693.

[28] C.F. Lam, T. Grkovic, A.N. Pearce, B.R. Copp, Investigation of the electrophilic reactivity of the cytotoxic marine alkaloid discorhabdin B, Org. Biomol. Chem. 10 (2012) 3092-3097.

[29] BRENDA: The comprehensive enzyme information system. http://www.brenda-enzymes.org/enzyme.php?ecno=3.1.1.7, 2016 (accessed 20.10.16).

[30] I. Orhan, M. Kartal, Y. Kan, B. Sener, Activity of essential oils and individual components against acetyl- and butyrylcholinesterase, Z. Naturforsch. C 63 (2008) 547-553.

[31] I. Orhan, F. Tosun, B. Sener, Coumarin, anthroquinone and stilbene derivatives with anticholinesterase activity, Z. Naturforsch. C 63 (2008) 366-370.

[32] J.D. Morrison, The generation of nerve and muscle repetitive activity in the rat phrenic nerve-diaphragm preparation following inhibition of cholinesterase by ecothiopate. Br. J. Pharmacol. 60 (1977) 45-53.

[33] A.L. Clark, F. Hobbiger, Twitch potentiation by organophosphate anticholinesterases in rat phrenic nerve diaphragm preparations. Br. J. Pharmacol. 78 (1983) 239-246.

[34] F. Bosch, M. Morales, A. Badia, J.E. Baños, Effects of velnacrine, tacrine and physostigmine on tetanic twitch responses at the rat neuromuscular junction. Eur. J. Pharmacol. 222 (1992) 163-166.

[35] C.C. Chang, S.J. Hong, J.L. Ko, Mechanisms of the inhibition by neostigmine of tetanic contraction in the mouse diaphragm. Br. J. Pharmacol. 87 (1986) 757-762.

[36] D. Kersken, B. Feldmeyer, D. Janussen, Sponge communities of the Antarctic Peninsula - influence of environmental variables on species composition and richness, Polar Biol. 39 (2016) 851-862.

[37] G.L. Ellman, K.D. Courtney, V. Andres, R.M. Featherstone, A new and rapid colorimetric determination of acetylcholinesterase activity, Biochem Pharmacol. 7 (1961) 88-95.

[38] M. F. Sanner, Python: a programming language for software integration and development, J Mol. Graphics Mod. 17 (1999) 57-61.

[39] O. Trott, A.J. Olson, Software news and update AutoDock Vina: improving the speed and accuracy of docking with a new scoring function, efficient optimization, and multithreading, J. Comp. Chem. 31 (2010) 455-461.

[40] J. Cheung, E.N. Gary, K. Shiomi, T.L. Rosenberry, Structures of human acetylcholinesterase bound to dihydrotanshinone I and territrem B show peripheral site flexibility, Med. Chem. Lett. 4 (2013) 1091-1096.

[41] H.M. Greenblatt, G. Kryger, T.T. Lewis, I. Silman, J.L. Sussman, Structure of acetylcholinesterase complexed with (−)galantamine at 2.3 Å resolution, FEBS Lett. 463(1999) 321-326.

[42] R.A. Laskowski, M.B. Swindells, LigPlot+: multiple ligand–protein interaction diagrams for drug discovery, J. Chem. Inf. Model. 51(2011) 2778-2786.

[43] Y. Zhang, J. Skolnick, TM-align: a protein structure alignment algorithm based on the TM-score, Nucl. Acid Res. 33(2005) 2302-2309.

Supplementary Material

Discorhabdin alkaloids from Antarctic *Latrunculia* spp. sponges as a new class of cholinesterase inhibitors

Tanja Botić[a], Andrea Defant[b], Pietro Zanini[b], Monika Cecilija Žužek[c], Robert Frangež[c], Dorte Janussen[d], Daniel Kersken[d], Željko Knez[a], Ines Mancini*[b], Kristina Sepčić*[e]

[a]Laboratory for Separation Processes and Product Design, Faculty of Chemistry and Chemical Engineering, University of Maribor, Smetanova 17, 2000 Maribor, Slovenia

[b]Laboratory of Bioorganic Chemistry, Department of Physics, University of Trento, via Sommarive, 14, I-38123 Povo-Trento, Italy

[c]Institute of Preclinical Sciences, Veterinary Faculty, University of Ljubljana, Gerbičeva 60, Slovenia

[d]Marine Zoology Department, Senckenberg Research Institute and Nature Museum, Senckenberganlage 25, D-60325 Frankfurt am Main, Germany

[e]Department of Biology, Biotechnical Faculty, University of Ljubljana, Večna pot 111, 1000 Ljubljana, Slovenia

^{1}H-NMR spectrum of the pure (+)-discorhabdin G (**1**) in CD_3OD (400 MHz).

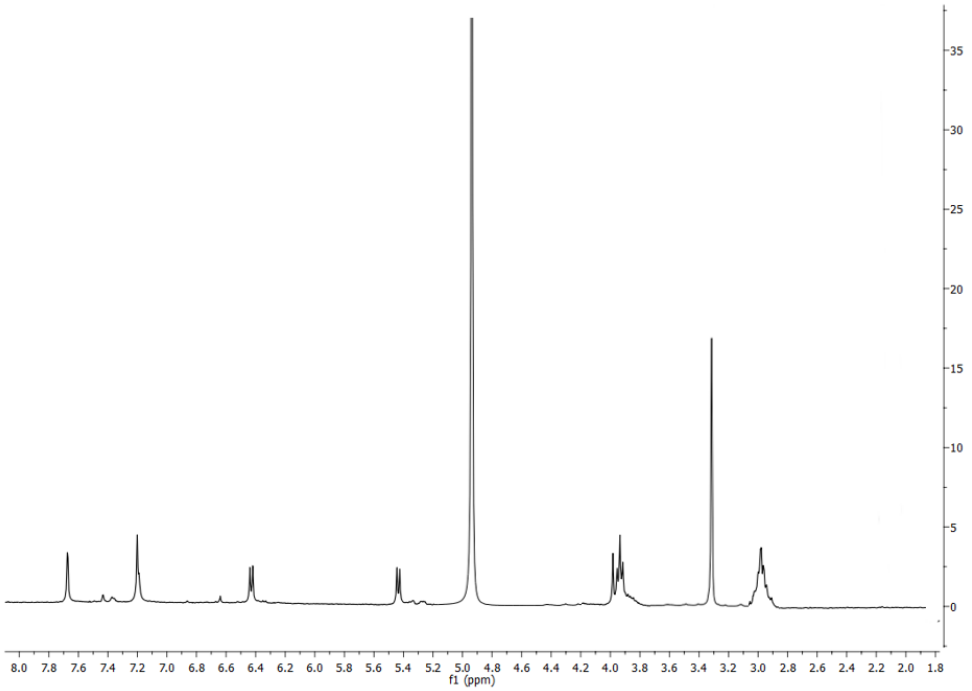

^{13}C-NMR spectrum of the pure (+)-discorhabdin G (**1**) in CD_3OD (100 MHz).

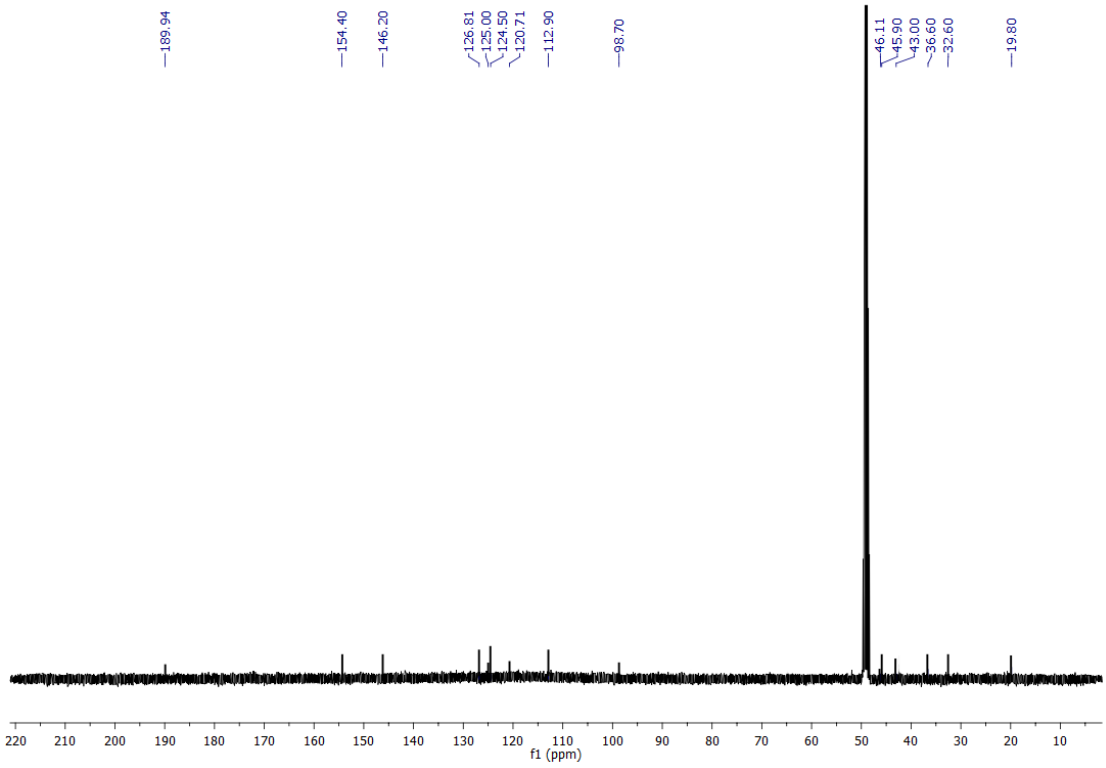

^{1}H-NMR spectrum of the pure (-)-14-bromo-3-dihydro-7,8-dehydro-discorhabdin C (**2**) in CD_3OD (400 MHz).

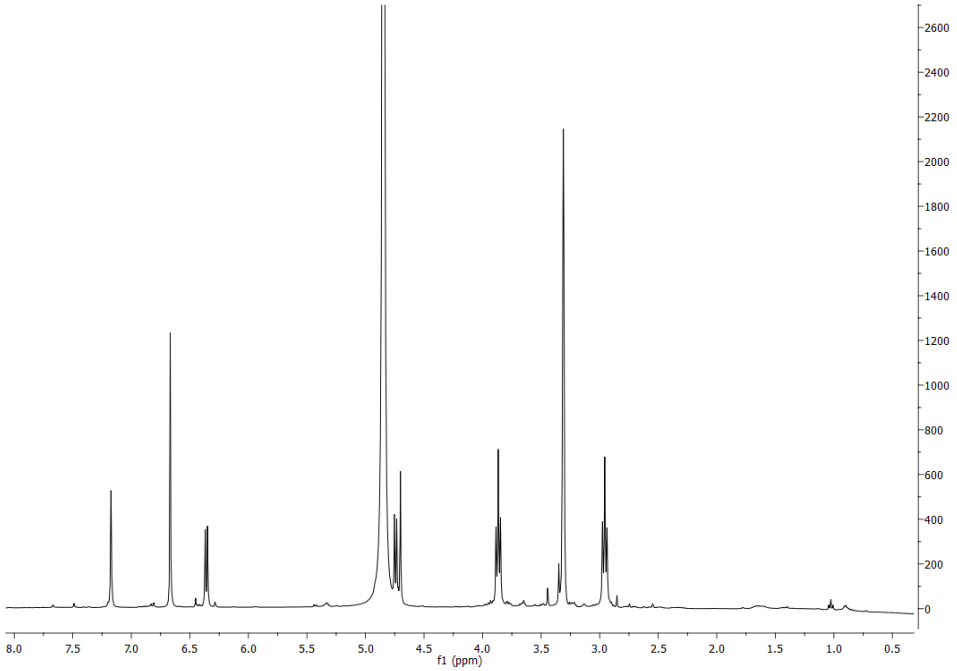

^{13}C-NMR spectrum of the pure (-)-14-bromo-3-dihydro-7,8-dehydro-discorhabdin C (**2**) in CD_3OD (100 MHz).

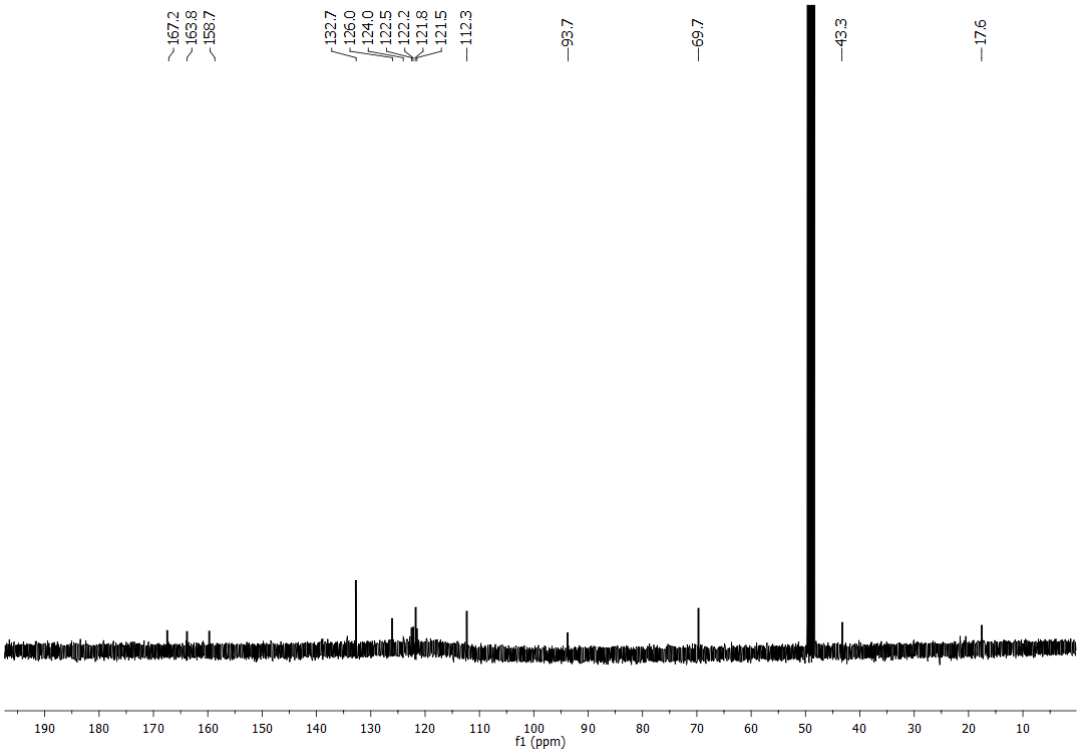

^{1}H-NMR spectrum of the pure (+)-discorhabdin B (**3**) in CD_3OD (400 MHz).

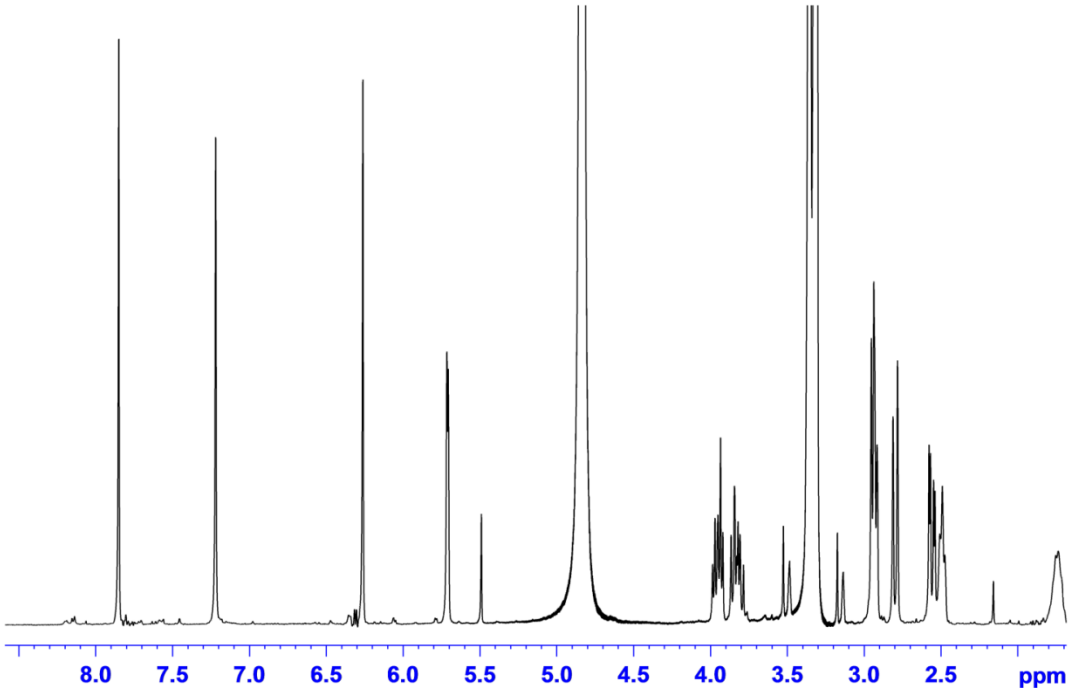

^{13}C-NMR spectrum of the pure (+)-discorhabdin B (**3**) in CD_3OD (100 MHz).

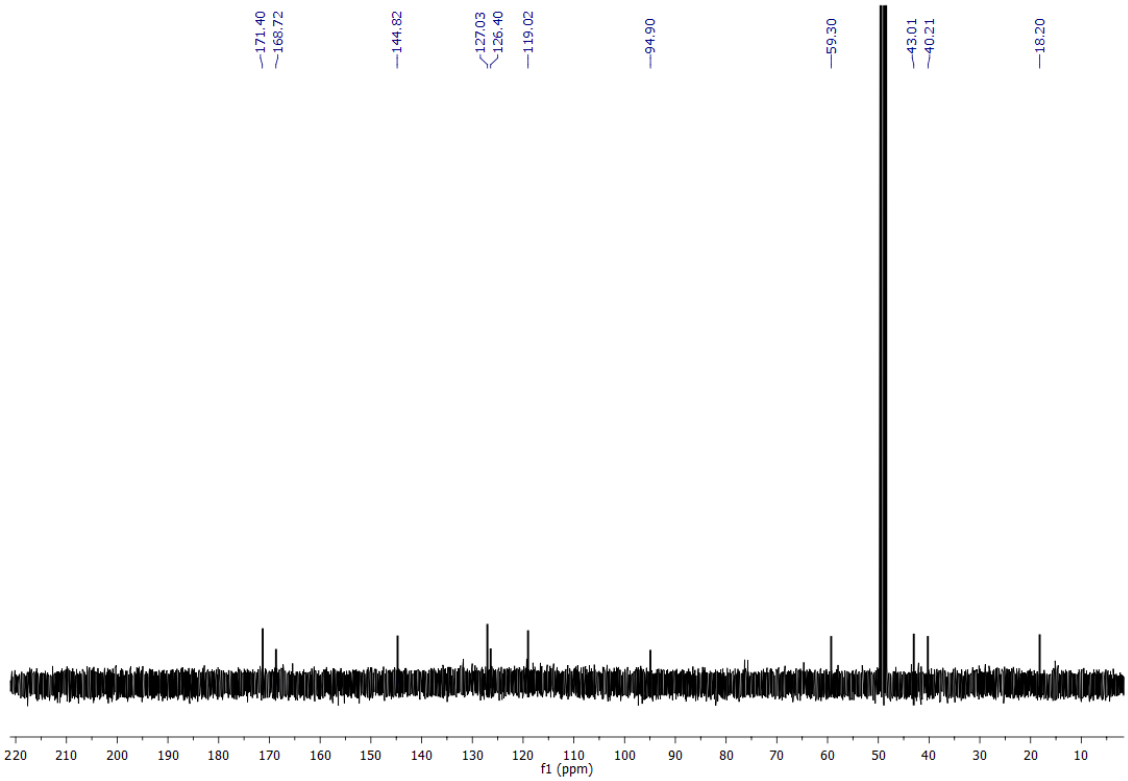

^{1}H-NMR spectrum of the pure (-)-discorhabdin L(**4**) in CD_3OD (400 MHz).

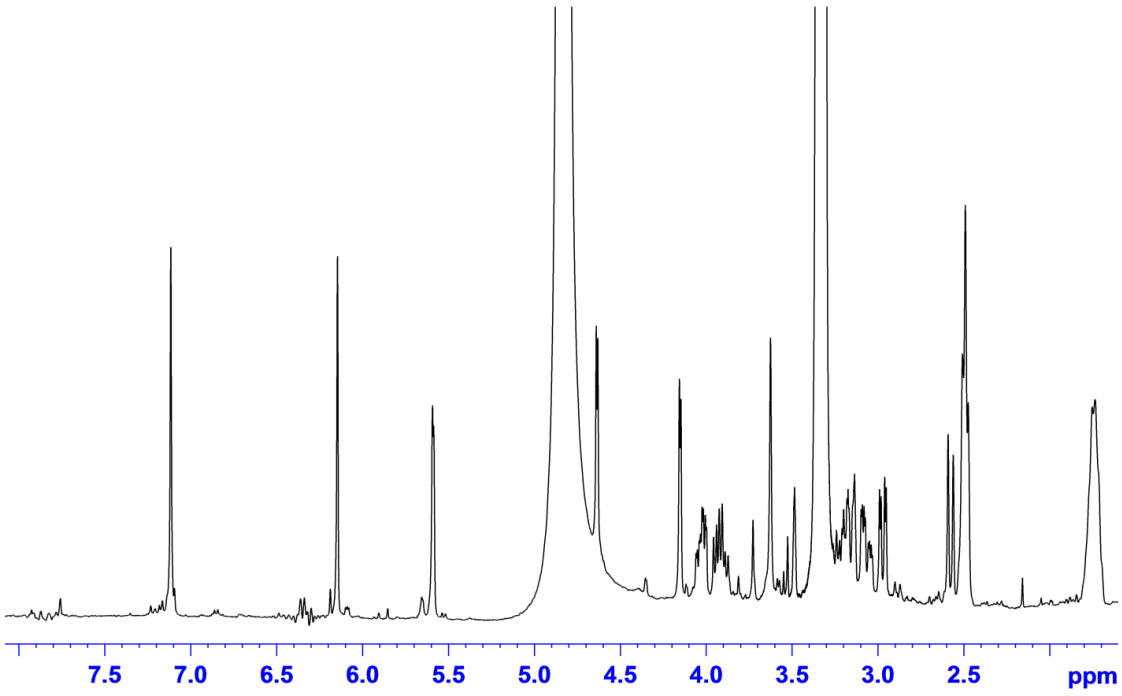

^{13}C-NMR spectrum of the pure (-)-discorhabdin L(**4**) in CD_3OD (100 MHz).

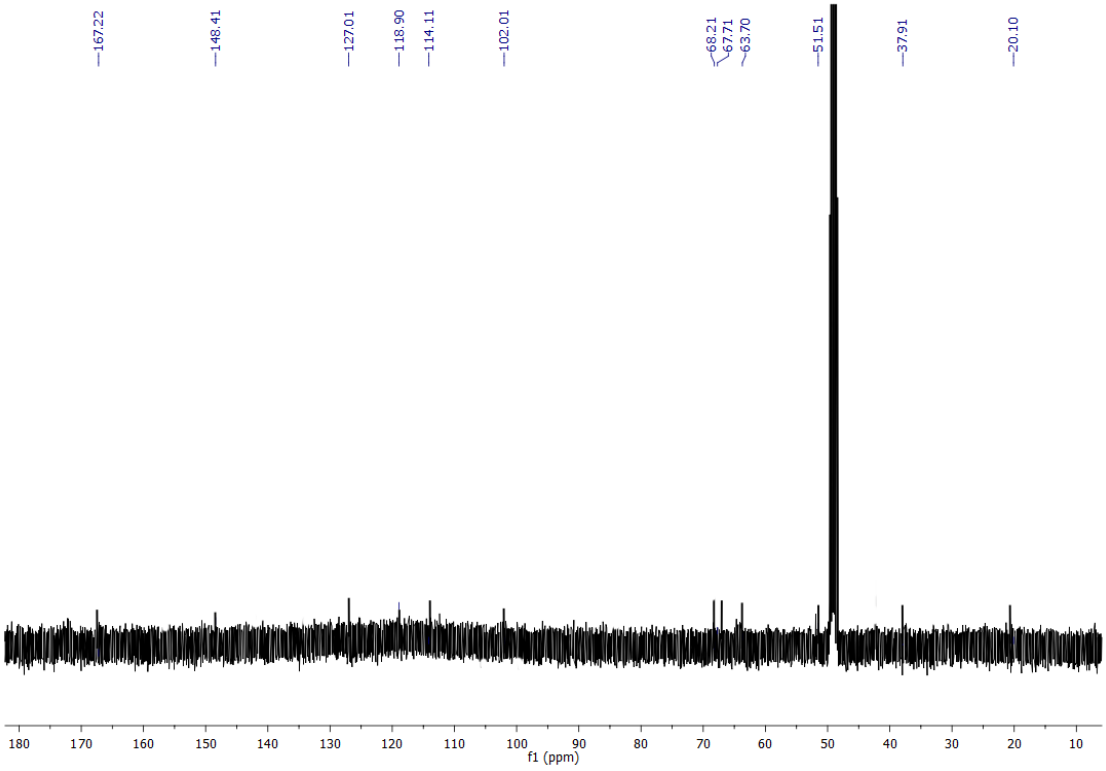

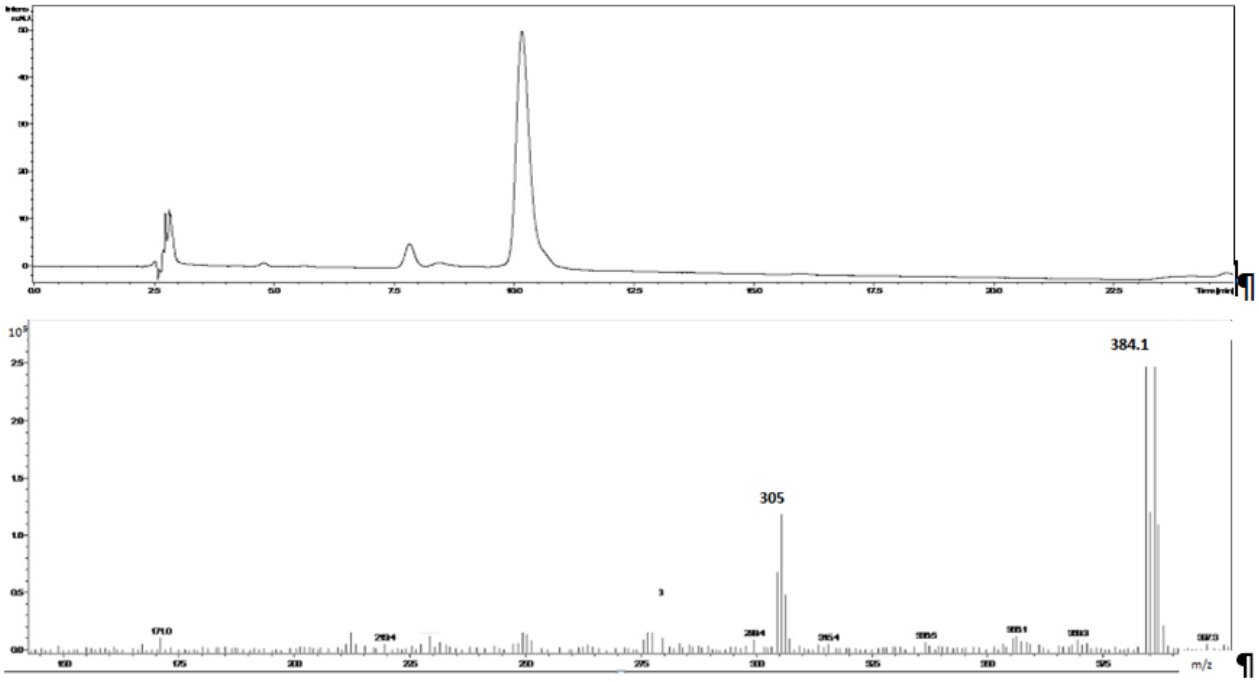

Fig. S1. LC-ESIMS analysis of the HPLC purified (+)-discorhabdin G trifluoroacetate salt (**1**), using a Lichrospher CN column and MeOH /H_2O/ 1% TFA as gradient mobile phase; Top: total ion chromatogram, Bottom: ESI-MS spectrum, recorded in positive ion mode for the peak at 10.1 min, with the M^+ signal at *m/z* 384/386.

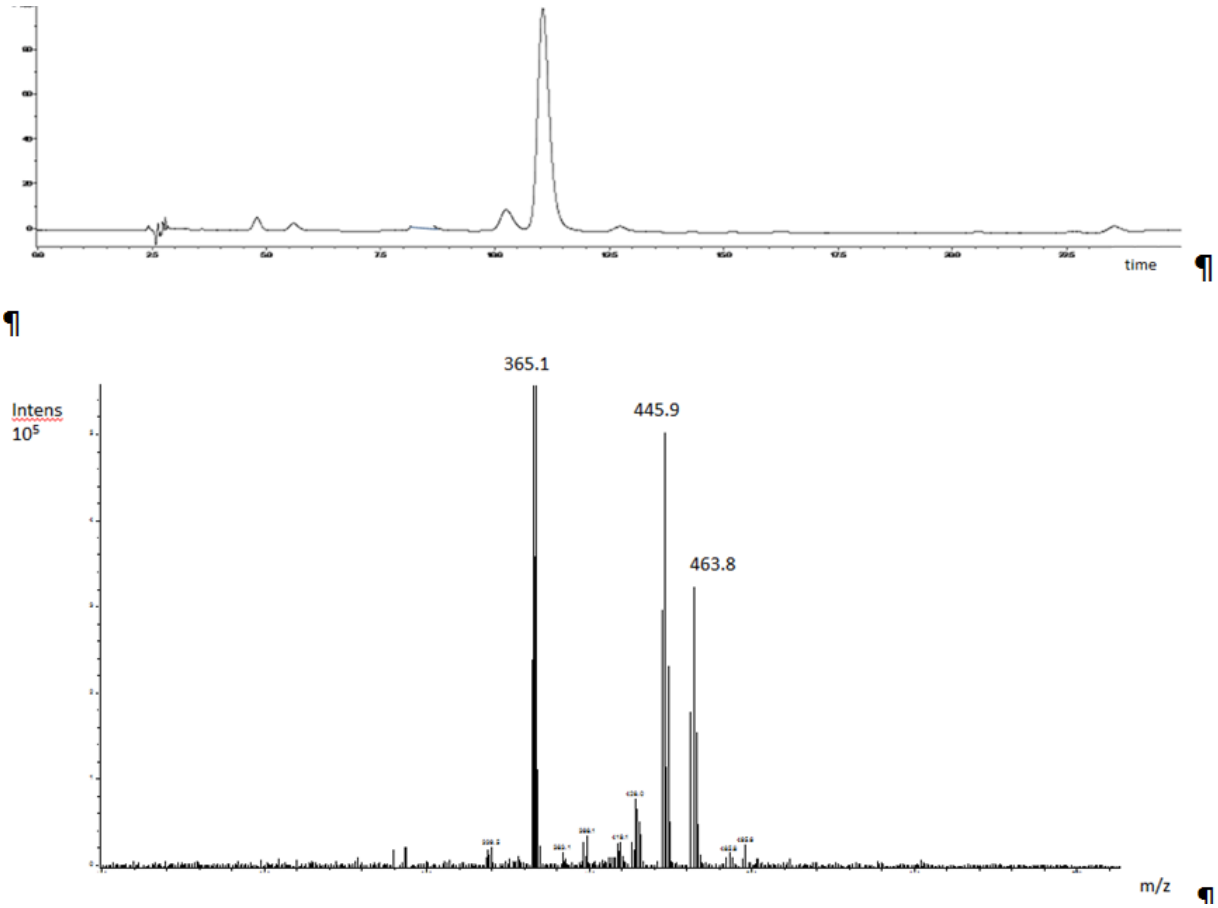

Fig. S2. LC-ESIMS analysis of the HPLC purified (-)-3-dihydro-7,8-dehydro-discorhabdin C trifluoroacetate salt (**2**), using a Lichrospher CN column and MeOH /H_2O/ 1% TFA as gradient mobile phase; Top: total ion chromatogram, Bottom: ESI-MS spectrum, recorded in positive ion mode for the peak at 11.1 min, with the M^+ signal at *m/z* 462/464/466.

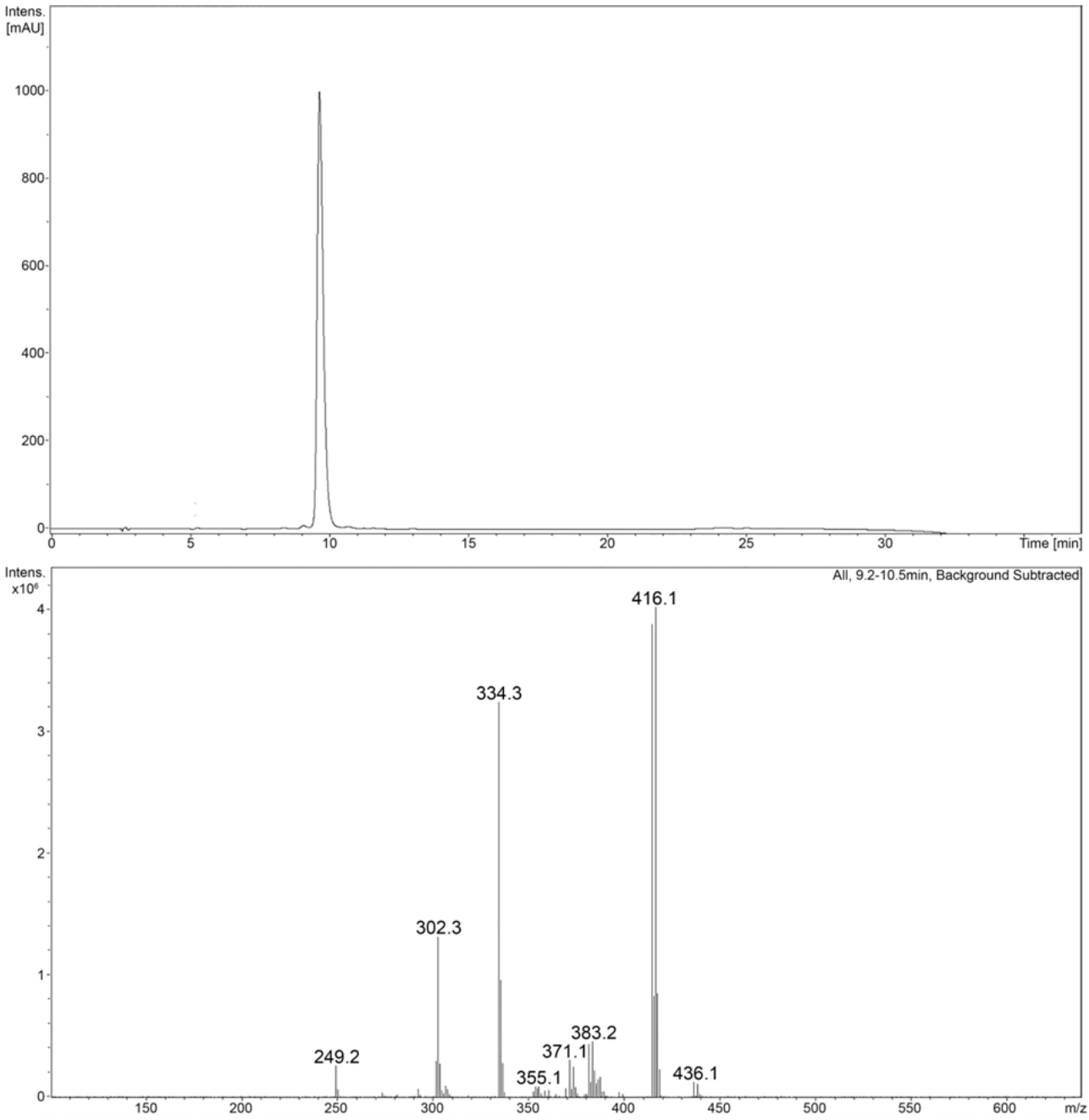

Fig. S3. LC-ESIMS analysis of the HPLC purified (+)-discorhabdin B trifluoroacetate salt (**3**) using a Lichrospher CN column and MeOH /H_2O/ 1% TFA as gradient mobile phase ; Top: total ion chromatogram, Bottom: ESI-MS spectrum, recorded in positive ion mode, corresponding to the peak at 9.7 min, with the M^+ signal at *m/z* 414/416.

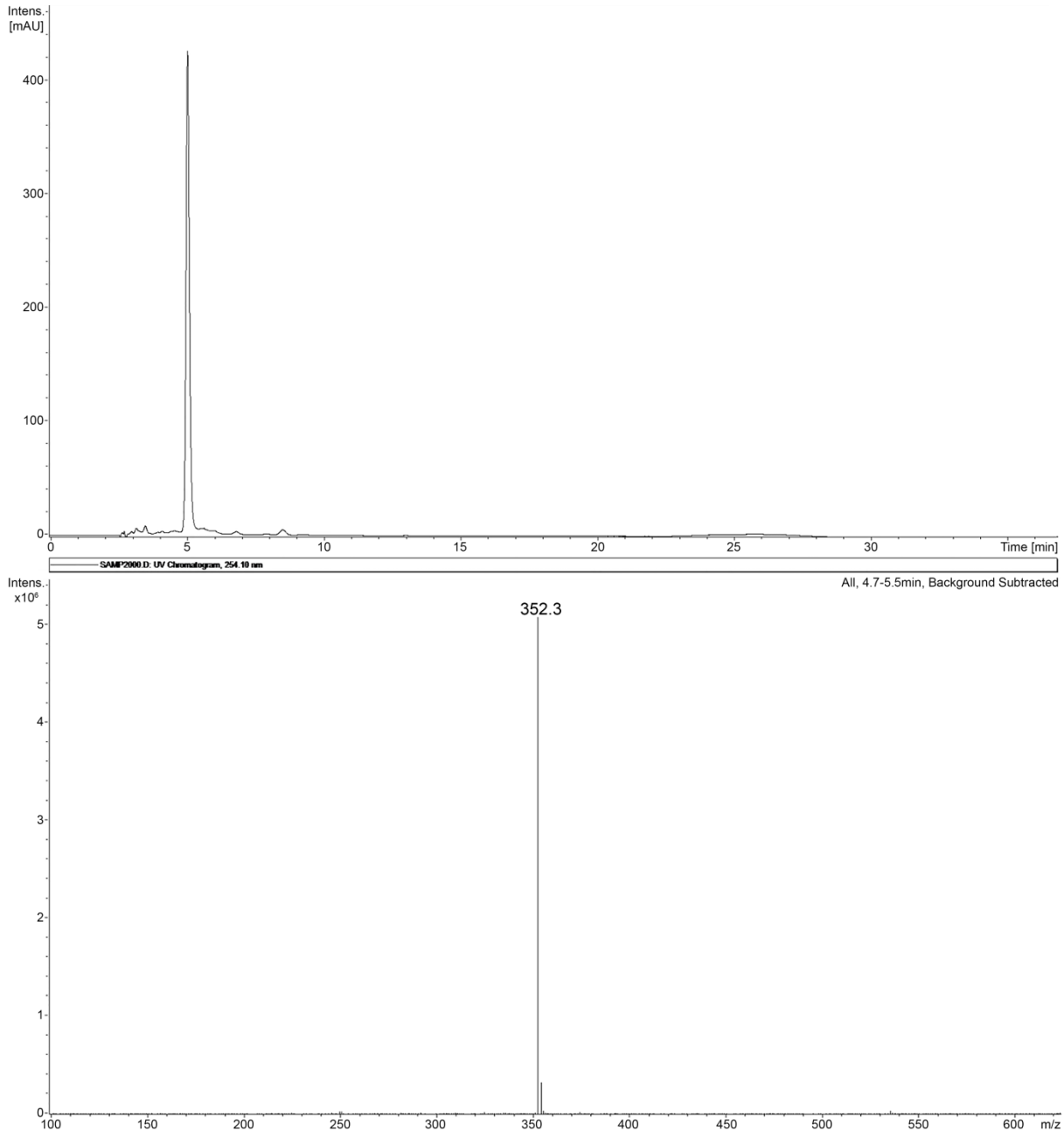

Fig. S4. LC-ESIMS analysis of the HPLC purified (-)-discorhabdin L trifluoroacetate salt (**4**) using a Lichrospher CN column and MeOH /H_2O/ 1% TFA as gradient mobile phase; Top: total ion chromatogram, Bottom: ESI-MS spectrum, recorded in positive ion mode, corresponding to the peak at 5.0 min, with the M^+ signal at *m/z* 352.

(":" denotes aligned residue pairs of d < 5.0 A, "." denotes other aligned residues)

```
DPQLLVRVRGGQLRGIRLKAPGGPVSAFLGIPFAEPPVGSRRFMPPEPKRPWSGVLDATTFQNVCYQYVDTLYPGFEGTEMWNPNRELSEDCLYLNVWTPYPRP
 ::::::::::::::::::::.:::::::::::::::::::::::::::::::::::::::::::::::::::::::::::::::::::::::::::::::::::
-SELLVNTKSGKVMGTRVPVLSSHISAFLGIPFAEPPVGNMRFRRPEPKKPWSGVWNASTYPNNCQQYVDEQFPGFSGSEMWNPNREMSEDCLYLNIWVPSPRP

ASPTPVLIWIYGGGFYSGAASLDVYDGRFLAQVEGAVLVSMNYRVGTFGFLALPGSREAPGNVGLLDQRLALQWVQENIAAFGGDPMSVTLFGESAGAAS
 :::::::::::::::::::::::::::::::::::::::::::::::::::::::::::::::::::::::::::::::::::::::::::::::::::::::
-KSTTVMVWIYGGGFYSGSSTLDVYNGKYLAYTEEVVLVSLSYRVGAFGFLALHGSQEAPGNVGLLDQRMALQWVHDNIQFFGGDPKTVTIFGESAGGAS

SVGMHILSLPSRSLFHRAVLQSGTPNGPWATVSAGEARRRATLLARLVGCPPGGAGGNDTELIACLRTRPAQDLVDHEWHVLPQESIFRFSFVPVVDGDFLSD
::::::::::::::::::::::::::::::::::::::::::::::::::::::::::::::::::::::::::::::::::::::::::::::::::::::::
SVGMHILSPGSRDLFRRAILQSGSPNCPWASVSVAEGRRRAVELGRNLNCN---LN-SDEELIHCLREKKPQELIDVEWNVLPFDSIFRFSFVPVIDGEFFPTS

PEALINTGDFQDLQVLVGVVKDEGSYFLVYGVPGFSKDNESLISRAQFLAGVRIGVPQASDLAAEAVVLHYTDWLHPEDPTHLRDAMSAVVGDHNVVCPVAQ
::::::::::.:::::::::::::::::::::::::::::::::::::::::::::::::::::::::::::::::::::::::::::::::::::::::::
LESMLNSGNFKKTQILLGVNKDEGSFFLLYGAPGFSKDSESKISREDFMSGVKLSVPHANDLGLDAVTLQYTDWMDDNNGIKNRDGLDDIVGDHNVICPLMH

LAGRLAAQGARVYAYIFEHRASTLTWPLWMGVPHGYEIEFIFGLPLDPSLNYTTEERIFAQRLMKYWTNFARTGDPNDPRDSKSPQWPPYTTAAQQYVSL
::::::::::::::::::::::::::::::::::::::::::::::::::::::::::::::::::::::::::::::::::::::::::::::::::::::::
FVNKYTKFGNGTYLYFFNHRASNLVWPEWMGVIHGYEIEFVFGLPLVKELNYTAEEEALSRRIMHYWATFAKTGNPNE-P----SKWPLFTTKEQKFIDL

NYTTEERIFAQRLMKYWTNFARTGDPNDPRDSKSPQWPPYTTAAQQYVSLNLKPLEVRRGLRAQTCAFWNRFLPKLLSAT
::::::::::::::::::::::::::::::::: :    ::::::::::::::::::::::::::::::::::::::::::::::::::
NYTAEEEALSRRIMHYWATFAKTGNPNE-P----SKWPLFTTKEQKFIDLNTEPMKVHQRLRVQMCVFWNQFLPKLLNAT
```

Aligned length= 528, RMSD= 0.97, Seq_ID=n_identical/n_aligned= 0.595; TM-score= 0.96775 (if normalized by length of Chain_1); TM-score= 0.98772 (if normalized by length of Chain_2).

Fig. S5. Comparison of the three-dimensional representations of sting ray (*Tetronarce californica*) AChE (PDB ID: 1DX6; violet) with electric eel AChE (PDB ID: 1C2O; orange) using the TM-alignment, with the obtained result. The amino acidic residues in the active sites of both AChEs are marked in red.

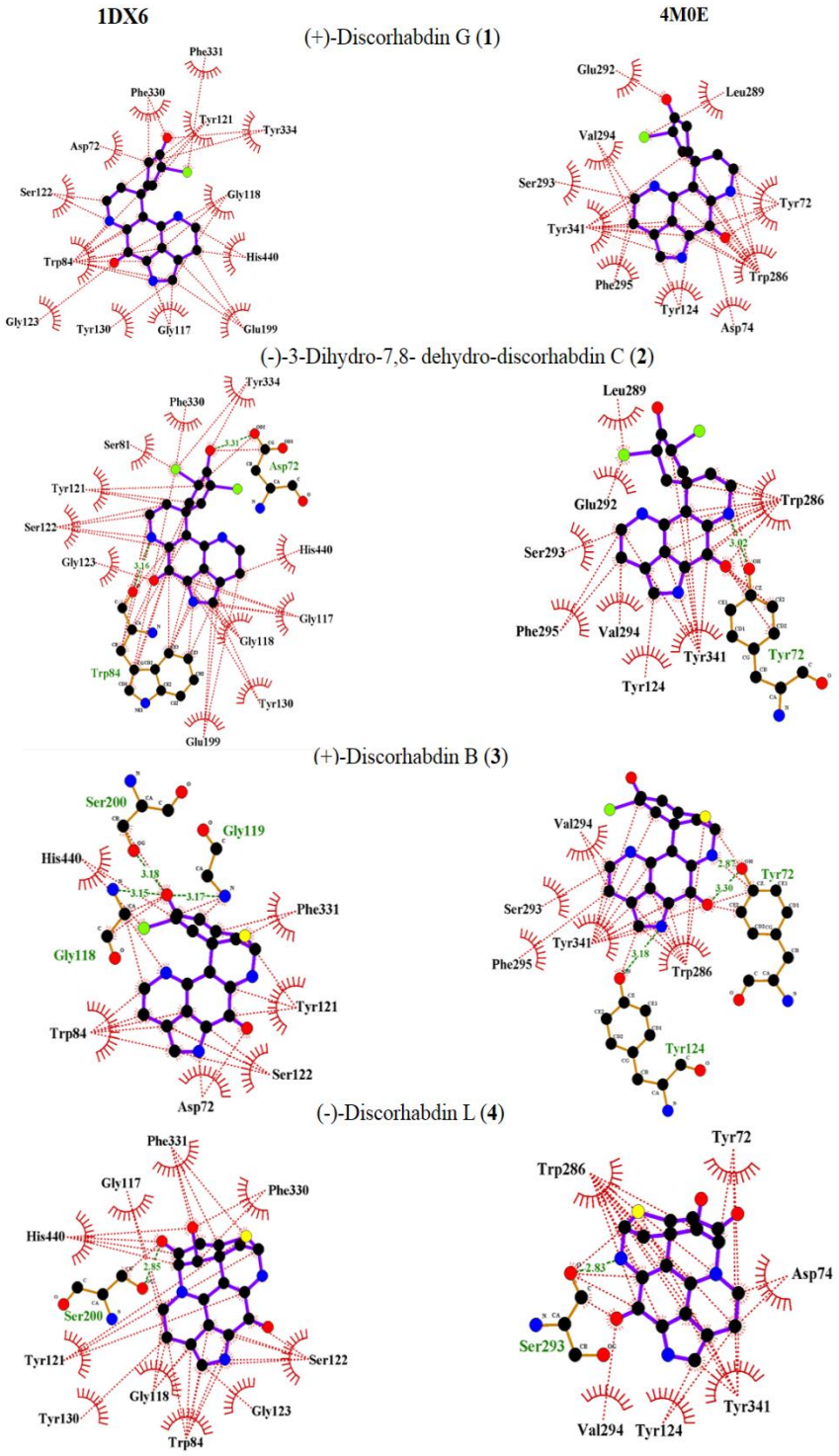

Fig. S6. Comparisons of the two-dimensional representations for the interactions of the discorhabdins **1-4** with sting ray (*Tetronarce californica*) AChE (PDB ID: 1DX6) and human *Homo sapiens* AChE (PDB ID: 4MOE) by docking calculations, with H-bonds indicated.

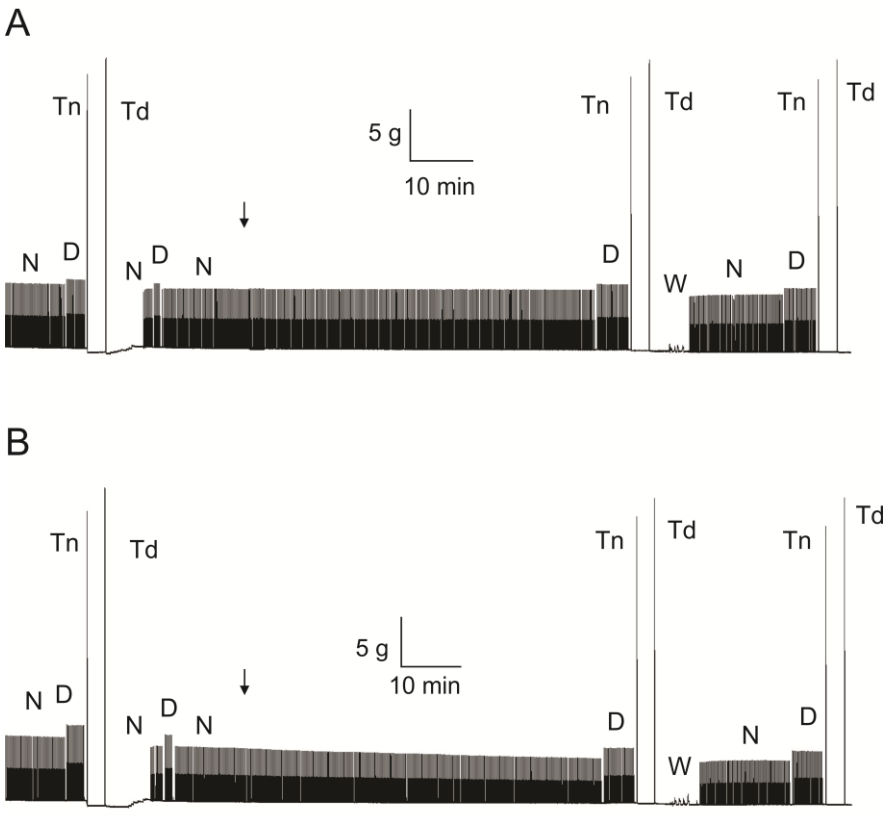

Fig. S7. Effects of discorhabdin G (**1**) on contractions in the isolated mouse hemidiaphragm preparation. (A) Representative control trace. Arrow, superfusion of 0.035% (v/v) ethanol solution (final concentration). (B) In the presence of 8.43 μM discorhabdin G. N, nerve-evoked muscle contraction; D, directly elicited muscle contraction; Tn, nerve-evoked tetanic contraction; Td, directly elicited tetanic contraction; W, washout.